INVESTIGATION OF BROADBAND OVER POWER LINE CHANNEL CAPACITY OF SHIPBOARD POWER SYSTEM CABLES FOR SHIP COMMUNICATIONS NETWORKS

A Thesis

by

AYORINDE AKINNIKAWE

Submitted to the Office of Graduate Studies of
Texas A&M University
in partial fulfillment of the requirements for the degree of

MASTER OF SCIENCE

December 2008

Major Subject: Electrical Engineering

INVESTIGATION OF BROADBAND OVER POWER LINE CHANNEL CAPACITY OF SHIPBOARD POWER SYSTEM CABLES FOR SHIP COMMUNICATIONS NETWORKS

A Thesis

by

AYORINDE AKINNIKAWE

Submitted to the Office of Graduate Studies of
Texas A&M University
in partial fulfillment of the requirements for the degree of

MASTER OF SCIENCE

Approved by:

Chair of Committee,	Karen L. Butler-Purry
Committee Members,	B. Don Russell
	Deepa Kundur
	Christine Ehlig-Economides
Head of Department,	Costas Gheorghiades

December 2008

Major Subject: Electrical Engineering

ABSTRACT

Investigation of Broadband over Power Line Channel Capacity of Shipboard Power System Cables for Ship Communications Networks. (December 2008)

Ayorinde Akinnikawe, B.S., Wichita State University

Chair of Advisory Committee: Dr. Karen L. Butler-Purry

Broadband over Power Line (BPL) technology has garnered significant attention lately due to recent advancements in solid state technologies and channel coding schemes. The successful application of BPL technology for in-home automation and networking has led to suggestions of applying BPL in other systems including ships. The application of BPL technology using the Shipboard Power System (SPS) as a potential communications network for ship automation systems has been proposed, to achieve recent U.S. Navy ship management concepts geared toward reducing ship manning while improving operational efficiency. This thesis presents an analytical model developed to examine the channel response characteristics and estimated throughput capacity of SPS cables. The work used a multiconductor transmission line theory based approach to model the channel response of SPS distribution lines and estimated the channel throughput capacity using a "water-filling" communication technique. This work found that BPL using the SPS holds a strong potential for use as a communications network for ship communication systems.

DEDICATION

To my parents, siblings, and daughter Ayanna.

Thank you for your continued support, love, prayers and

joy you have given me.

ACKNOWLEDGEMENTS

First and foremost, I wish to thank God for all his blessings and enduring mercy afforded to me throughout my life and especially my college years in a foreign country from my birth country of Nigeria. I ask that the Lord continue to watch over me and lead me in the right path through the rest of my life. I also wish to thank my parents, Mr. and Mrs. F.A. Akinnikawe, for all your love, financial and moral support that has been instrumental to my every success and achievements. May the Lord in his infinite mercy give you long life and good health to enjoy the fruits of your labor. I wish to thank my girl friend, Erin, for her support and assistance. Erin, thank you for your patience, understanding, and care of our daughter, Ayanna, while I was completing my master's degree.

I thank my advisor, Dr. Karen L. Butler-Purry for her guidance and support throughout my program. I learned many invaluable professional and life lessons from you. I give special thanks to Dr. Christen Ehlig-Economides for your support that made my master's degree possible. I would also like to thank my other committee members, Dr. B. Don Russell and Dr. Deepa Kundur, for taking the time and effort to serve on my committee. My gratitude goes to the ECE staff members especially Tammy, Jeanie, Gayle and Linda for all their help. Finally, but not in the least, I wish to thank my colleagues in the Power Systems Automation Laboratory for the friendship and support. Fabian, LT, Gayatri, Tushar and Ebony, special thanks to you all for helping me in various capacities towards the completion of my master's degree.

NOMENCLATURE

AC	Alternating Current
ATG	Auxiliary Turbine Generator
BPL	Broadband over Power Lines
DC	Direct Current
EMI	Electro-Magnetic Interference
IPS	Integrated Power System
LAN	Local Area Network
MTG	Main Turbine Generator
MTL	Multiconductor Transmission Line
NGIPS	Next Generation Integrated Power System
NM	Non-Magnetic
PLC	Power Line Communication
RFI	Radio Frequency Interference
SPS	Shipboard Power System

TABLE OF CONTENTS

Page

Page

LIST OF FIGURES

Page

Page

LIST OF TABLES

Page

1. INTRODUCTION

1.1 INTRODUCTION

Current ships use fiber, ethernet, and wireless technologies for their Local Area Networks (LAN). The LANs are used for interior communication and automation system networks on the ship [1, 2]. The fiber and ethernet networks are made up of hundreds of kilometers of cabling [3] that add considerable weight and increase overall cost of the ship. Conversely, ship wireless LAN coverage is limited by the ship hull, which is made of thick metal sheets [4].

An alternative communications technology currently being considered for implementation in ships is Broadband over Power Lines (BPL). BPL is a process of using power lines for high-speed data transmission. Electric power signals operate at low frequencies of 50 or 60Hz, and at 400Hz in certain systems of some ships. The low frequencies leave ample space in the higher frequency spectrum of the power lines for transmitting data streams [5]. In BPL, radio frequency signals at high frequencies are superimposed onto the power line for data transmission. The technique of transmitting data over power lines was first used as early as the 1930s by utilities for remote control of some of their breakers and switches. These applications, which are still in use today, require relatively low speed (<30kbps) data communications [6].

This thesis follows the style of *IEEE Transactions on Power Systems.*

The power network, which was optimized to operate at 50 or 60Hz, has inherent noise, high reflection coefficient, and severe attenuation that make it difficult to send higher frequency signals through it. However, recent technological advances in solid state technology and signal coding methods make it possible to use a higher frequency band to transmit data faster (>2Mbps) over power lines [7, 8].

Given the ubiquity of the Shipboard Power System (SPS) cables within U.S. Navy ships, power line paths that connect components in different regions of the ship exist. As such, the SPS cable network could be used as the communications medium for various ship automation systems. However, the SPS is comprised of several other components in addition to the power cables. These additional components include transformers, power electronic converters, bus transfers, circuit breakers, and switches at high, medium, and low voltage levels. Where it is known that high-frequency signals are severely attenuated by transformers [9, 10], the effect of passing BPL signals through the other components such as power converters and bus transfers has not been studied. Therefore, there is a need to determine if the application of BPL technology for automation in Navy ships is feasible.

In related work, the authors of [3] measured the point-to-point channel frequency response of cruise ship power lines and verified the feasibility of using BPL technology to transmit communication signals using the low-voltage (220V) lighting network in a typical cruise ship. In a similar manner, the authors of [11, 12] measured the transfer function parameters of cargo ship low-voltage power lines, with particular emphasis on the effect of armored and unarmored cables on the transfer function parameters. While

these efforts have attempted to measure the channel response characteristics of SPS cables, no analytical model has been developed for determining *a priori* the channel characteristics of ship power lines and other SPS components. Such a model will create a platform for the design, testing, and optimization of ship BPL communication systems prior to implementation.

In the work presented in this manuscript, an approach was developed for analytically determining the BPL channel response of the typical cable that might be found on the U.S. Navy next generation all-electric ship. Analytical approaches for determining the frequency response of residential/in-home power lines [6, 13-15] using Two-port network models were adapted to determine the frequency response of the ship cables. A "water-filling" communication technique was used to estimate the data capacity of the cables. The cables studied were marine standard cables based on the U.S. Navy (M24643) and IEEE 1580 specifications and approved by the American Bureau of Shipping (ABS) for use in ships. The cable sizes and types selected for this study were based on the conceptual voltage levels in the notional Next Generation Integrated Power System (NGIPS) ship power system.

1.2 ORGANIZATION OF THESIS

This thesis presents the research conducted to develop an analytical model for investigating the channel response characteristics of U.S. Navy ship distribution lines. Section 2 presents the literature review of BPL, past works conducted on BPL in ships as well as the motivation for this research work. Section 3 discusses ship automation

systems and the notional NGIPS architecture. The problem addressed in this work is also clearly stated in this section. In Section 4, the stepwise procedure for characterizing the ship cable channel response and throughput capacity is presented. The implementation of the developed model is discussed in Section 5 while Section 6 presents the simulation studies performed and their results. Finally, conclusions and future work is discussed in Section 7.

2. LITERATURE REVIEW

2.1 INTRODUCTION

In recent years, the advancement in broadband over power line technology and its perceived potential has lead to several studies been performed to determine its feasibility for use for communications in several systems, such as airplanes, cars, airport lighting systems, ships and space shuttles, that have pre-existing power cables. This section will briefly discuss the history of Broadband over Power Lines and some of the challenges still plaguing the technology. Some research that has been performed to investigate the feasibility of power-line communication/broadband over power line communications in ships will also be discussed.

2.2 BROADBAND OVER POWER LINES

Broadband over power lines (BPL) also known as Power Line Communications (PLC) is an advancement of a long existing technology, Power Line Carrier. Inherent in the name, BPL/PLC in simple terms is the use of existing power lines for streaming data signals (communications). The fundamental principle behind this is that electricity flows over the low-frequency (50 / 60 Hertz) portions of the power lines, leaving room in the higher frequency portions for data streams, as illustrated in Fig. 2.1 [5]. Power Line Carrier was originally proposed in the early 1800's and by 1838 the first remote electricity supply metering was proposed [16]. The first patents on power line signaling were proposed in the UK in 1897 and the technology used as early as the 1920's by

utilities such as the Electric Power Utility of London. Utilities early use of the power line communication technology was to remotely control some of its equipments including breakers and high voltage switches. This application of the technology only required the transfer of data at relatively low speeds of <30 kbps transfer rate and is still in use by several utilities today.

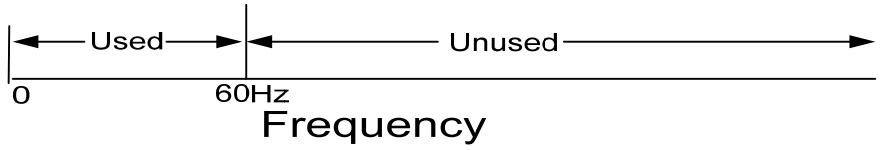

Fig. 2.1 Frequency Use of Power Line [5]

Earlier attempts to transfer data at higher speeds/frequencies over power lines proved to be unattainable as the electric grid was designed for optimal operation at low frequencies (50 / 60 Hz). This resulted in severe attenuation or signal blockage of high frequency signals by voltage regulators, circuit re-closers, transformers, and shunt capacitors. The inherently noisy nature of power line channel and high reflection coefficient of the distribution network due to signal reflection at branches and unmatched terminations, also increased the challenges of BPL/PLC [7].

The use of BPL/PLC technology has been experiencing significant attention lately due to a combination of factors such as the recent advances in solid state

integrated circuit technology, the development of improved signal modulation schemes, the liberalization of telecommunications and deregulation of electric utilities [16], coupled with the birth and growth of the internet and the increasing demand for communication networks for home and office automation, computer communications, security monitoring and several other applications [7]. This renewed interest stems partly from the desire to take advantage of the already extensive network infrastructure of the electric grid, which is estimated to have a worldwide coverage of around 90% [17]. If broadband communication services can be fully achieved using the power distribution network, a truly universal information superhighway with the capability of providing interconnection to every home, office and industry may be realized [16].

By the late 1980's, relatively sophisticated error control coding techniques within BPL/PLC modems were proposed [16]. Several spread-spectrum modulation schemes such as frequency shift keying(FSK), code-division multiple access(CDMA) and orthogonal frequency division multiplexing(OFDM) which are suitable for use on an inherently noisy channel were developed. These coding schemes were also found to be effective in overcoming some of the key challenges, including limited bandwidth - in comparison to fiber-optic links, high noise levels, uncertain and varying levels of impedance and attenuation [10]. This gave further impetus for additional research in the area. Advances made in the BPL/PLC industry have lead to the development of two spheres of the technology, In-Home BPL/PLC and Access BPL/PLC.

2.2.1 In Home BPL/PLC

In-home BPL, also referred to as in-building BPL/PLC, is a terminology used in the industry to refer to Broadband over Power Lines applications that use the existing electric power lines within a home, office or industrial building. In-home BPL/PLC has been in use since the 1980's [9] when power lines were used to connect computers and peripheral devices such as printers and plotters within an office building. It is currently the most developed of the two BPL technologies. Standardization by the HomePlug power Alliance (HomePlug 1.0, HomePlug AV) and the universal powerline association (UPA) has led to the commercial availability of several household appliances, such as the refrigerators, multi-media devices, coffee makers, and alarm clocks [18], that can communicate over the building power lines.

2.2.2 Access BPL/PLC

Access BPL/PLC, as the name implies, is the broadband over power line technology geared to serve as a last mile access technology for getting communication signals to the home, much like cable and Digital Subscriber Line (DSL), over the power distribution network. This feat is achieved by connecting the low to medium voltage distribution network to a communication backbone at the distribution transformer. The communication signal is then super-imposed onto the transmission lines as radio frequency signals between 1MHz to 100MHz [7]. Development and wide spread adoption of access BPL/PLC has been at a much slower pace than its in-home counterpart. This is mainly due to some challenges imposed by the transmission network, which was not designed for communication signals at high frequencies.

In a bid to validate the technology for commercial use as a last mile communication access medium, several field trials and pilot programs were run by/with electric supply companies and utilities in several European countries- notably in Spain, Portugal and France- as well as in Singapore and Hong Kong. However, several of these trials did not fare well. One of such was a trial in the Manchester Area between 1997 and 1999 by Norweb Networks and Norweb/United Utilities which was abandoned due to technical (mainly interference) and economical reasons [19]. Two of the key challenges (Technical and Economical challenges) facing the commercial deployment of access BPL/PLC will be briefly discussed here.

2.2.2.1 Technical Challenges

It has been proven in field studies that the existing access BPL/PLC technologies work. The question that remains unanswered is if it will work well in a full scale commercial deployment. BPL/PLC is a shared bandwidth technology and as such a bandwidth issue may arise in densely parked urban areas. Also, since power distribution cables were not designed to carry high frequency communication signals, some of the signals are radiated by the distribution cables – acting as an antenna – which leads to electromagnetic interference (EMI) and radio frequency interference (RFI) for other signals in the same spectrum as the BPL/PLC signal.

2.2.2.2 Economical Challenges

Economical challenge is one of the most severe challenges facing BPL/PLC today. One of the most alluring factors of the technology is that it uses the existing

electric distribution grid and as such does not require much initial capital investment for building a new network infrastructure. In reality though, partly due to the regulatory restrictions that require BPL/PLC signals to be transmitted using low power - in order to reduce EMI/RFI, coupled with the inherent noise and signal attenuation in the medium, the BPL/PLC signal requires the use of signal repeaters every few hundred yards [7]. With the use of complex spread spectrum coding techniques, the hardware required for BPL/PLC is also complex and as such expensive. These inherent costs may make it difficult for BPL/PLC to compete with existing DSL, wireless and cable services.

2.3 REVIEW OF EXISTING WORK ON BPL IN SHIPS

2.3.1 Cruise Ship

The authors of [3] performed experimental measurement of the channel response of the power-line communication channel of a typical cruise ship. In their work, they measured the power-line communication channel frequency response and background interference of the cruise ships lighting network. Inductive coupling was used to superimpose the power-line signal onto the lighting power cable and the channel frequency response was measured from 1-30MHz. In this manner, the authors of [3] were able to verify the feasibility of using the cruise ship power cables for power-line communication.

However, the ship power system considered in this work was comprised of several independent power generators for individual *fire zones.* This indicates some level of isolation of each zone from the other, which could prevent the use of this network for

ship-wide data transmission. Also, by using the lighting network, the system considered was limited to a single low voltage and cable size, thus not providing an insight into the effect of signal reflections that may occur due to the interconnection of different cable sizes along the communication path.

2.3.2 Cargo Ships

Similar to the work in [3], the authors of [11] and [12] performed a measurement analysis of ship power-line channels of cargo ships. However, in [11], the measurement analysis was performed, with a goal to develop a more suitable power-line transmission technique, by measuring the longitudinal conversion transfer ratio, longitudinal transfer ratio and transverse transfer ratio parameters of the low-voltage distribution lines in cargo ships. In [12], the authors of [11] advanced their work to consider the effect of cable armoring on the power-line channel response and the performance of different signal transmission modes.

2.4 MOTIVATION

To the best of the author's knowledge, no previous work has been done to develop an analytical model for determining the BPL/PLC channel response characteristics of SPSs. Such a model will create a platform for the design, testing, and optimization of ship BPL/PLC systems prior to implementation. Furthermore, an analytical model of the various components of a SPS will enable the analysis of the BPL/PLC channel response of SPS networks regardless of the topology of the SPS employed in different ships.

2.5 SUMMARY

In this section, a literature review on BPL/PLC was provided. The BPL/PLC concept was described and a brief history of the technology presented. Some recent advances, applications and challenges of BPL/PLC technology were also discussed. A review of existing research work on BPL/PLC in ships was also provided. The results of the review show that there is a need for more research to be done to determine *a priori* the BPL/PLC channel response characteristics of the different SPSs.

The section was concluded with a brief explanation of the motivation for performing this research work. In the next section, the problem formulation for this work will be discussed and then the specific scope of the work done in this research will be presented.

3. PROBLEM FORMULATION

3.1 INTRODUCTION

This section presents the formulation of the problem that this research aims to address. Considering the plethora of different ships and there respective SPSs, the BPL/PLC model developed in this work was based on the notional SPS topology of a class of U.S. Navy ships. In this work the notional SPS topology of the new NGIPS class surface combatant ships was used. The automation needs of these ships and a general description of the NGIPS topology is discussed. Finally, the work needed to develop the analytical model for characterizing the BPL/PLC channel response of the NGIPS system is presented and the specific focus of this work stated.

3.2 SHIP AUTOMATION SYSTEM

Naval ship systems such as the ship combat systems, navigation systems, power systems, and propulsion systems are made up of several components that may individually be located in different ship compartments, spread throughout the entire ship. The proper functioning of each of these systems is dependent on the performance of each individual component, thereby making it a challenging task to manually manage, monitor operational condition and maintain each system.

The propulsion system for instance, which is made up of several parts including generators, propeller motors, drive systems, propellers, rudders, and their associated controls, as shown in Fig. 3.1, is needed to provide sea surface movement of the ship, a

critical function for the survival of the ship and its crew. Automation of this system allows effective management and real time monitoring of the sub-systems and components thereby improving its availability. Hence, several ship systems have been automated to allow system operators to remotely and efficiently manage and monitor component status from central stations [1].

In present day naval ships, Shipboard propulsion engines, auxiliaries, electrical power generation and distribution systems are normally controlled from individual central stations called the engineering operator station (EOS) or machinery plant control and monitoring station (MPCMS) [1]. Other systems such as the combat, navigation, and safety systems are also monitored and controlled from central locations. Plans for future ships include the integration of these various separate control station to facilitate a streamlined control of all ship control systems from a central location to increase efficiency while reducing manning, without sacrificing functionality [20].

The remote monitoring and control of various ship systems require the implementation of reliable communication networks, which may comprise of multiple LANs connecting the various systems and a central control station as shown in Fig. 3.2, to transfer component parameter data and control data between the equipment and the central control station. Current ship LAN communication networks are fiber-optic or ethernet based [2, 21]. As such, hundreds of kilometers of fiber and Ethernet cables are used in the implementation of ship communication networks. Some of the issues that arise due to this include an increase in ship weight, cost of ship building, operation and

maintenance. The potential of using the existing shipboard power distribution system as the communication network for ship automation systems is being considered.

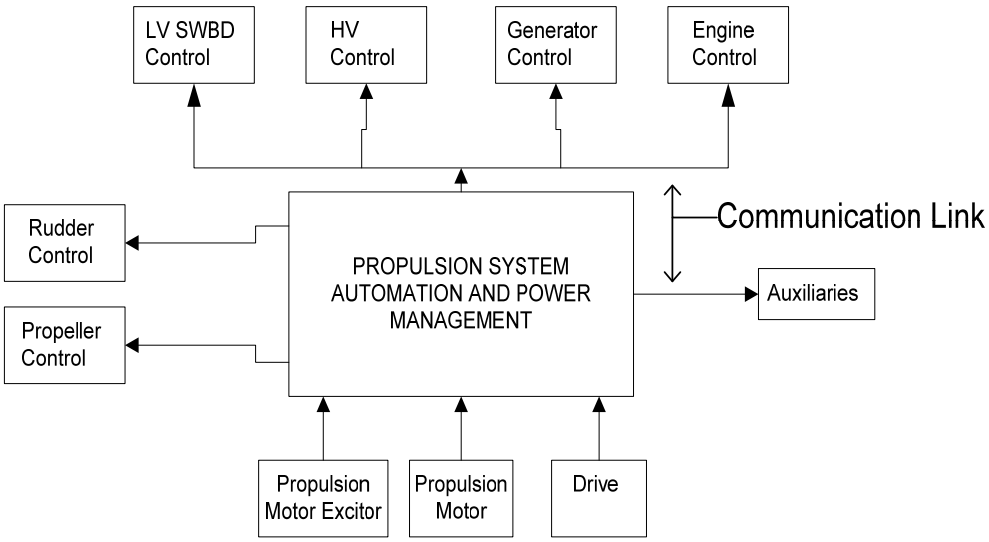

Fig. 3.1. Automation and Power Management –Electric Propulsion System [1]

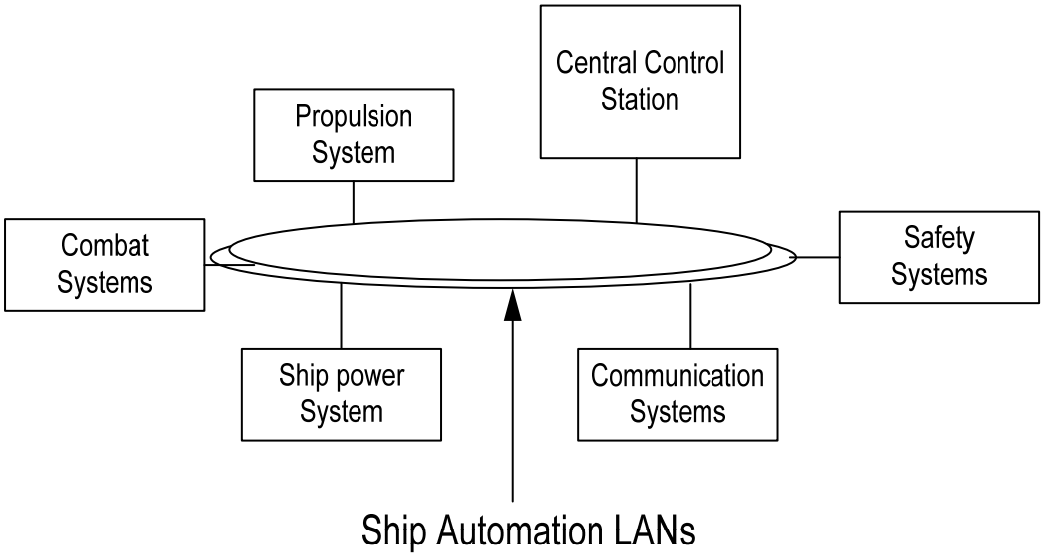

Fig. 3.2. Integrated Ship Automation System

3.3 SHIPBOARD POWER SYSTEM

The shipboard power system, like terrestrial power systems, can be divided into generation, transmission, and distribution networks. However, due to the relatively small size of the shipboard power system compared to terrestrial power systems, the transmission and distribution networks of a shipboard power system are very short and often simply referred to as a distribution network. In next generation ships, the Integrated Power System (IPS) architecture is to be used. This is the power system platform that forms the basic architecture for the future all-electric ships. The IPS uses an integrated platform to provide power for the entire ship, including propulsion and non-propulsion (ship service) systems [22], using the same rotating power generators unlike older generation ships that had a different power source for propulsion and non-propulsion systems.

A notional power system architecture for the NGIPS class ships was used for this research. The notional NGIPS is comprised of alternating current (AC) power generation and direct current (DC) power distribution parts as illustrated in Fig. 3.3. The notional NGIPS architecture has a total of four 13.8kV AC generators connected in a ring structure. There are two main generators, MTG1 and MTG2, with a power rating of 36MW each, and two auxiliary generators, ATG1 and ATG2, with power ratings of 4MW each. The generator voltage is stepped down to 4.16kV, using four 13.8kV/4.16kV Three-phase ship service transformers, which is the voltage level for the propulsion motors PM1 and PM2, and shore power (SP). There are four AC-to-DC power converter

modules (PCM-4), also connected to the 4.16kV buses of the ship distribution system, that are used to power each of the four zones in the ship.

The PCM-4's step down the 4.16kV AC power from the ring system and convert it to DC at 1kV. The 1kV DC is stepped down to 375V DC, 650V DC, and 800V DC by the PCM-1's, which perform DC-DC conversion, to serve the loads within each zone. . The 375V DC and 650V DC output of the PCM-1 is used to supply the lumped DC load centers (L_{DC}) in each zone, while the 800V DC output of the PCM-1 is used to supply the lumped AC load centers (L_{AC}) in each zone via a PCM-2, which performs 800V DC to 450V AC conversion. Protective devices and switches are not shown in Fig. 3.3.

In order to analyze the potential communication capability of the power system of the NGIPS for use as an automation communication channel that will enable remote monitoring and control of various ship components from central locations, it is necessary to determine the communication characteristics of the various components, such as circuit breakers, bus transfers, transformers, switches, power converter modules, and cables, that make up the NGIPS system. Other factors, such as ship reconfiguration, inherent noise in the ship power system, and electromagnetic interference issues, also need to be considered. The scope of this research was to analytically model the data capacity characteristics of the power cables in the notional NGIPS.

NGIPS Legend	
PCM-4	4.16kV – 1kV AC-DC
PCM-1	1kV-375/650/800V DC-DC
PCM-2	800V – 450V DC-AC
L_{DC}	Lumped DC Loads
L_{AC}	Lumped AC Loads
PM	Propulsion Module
SP	Shore Power

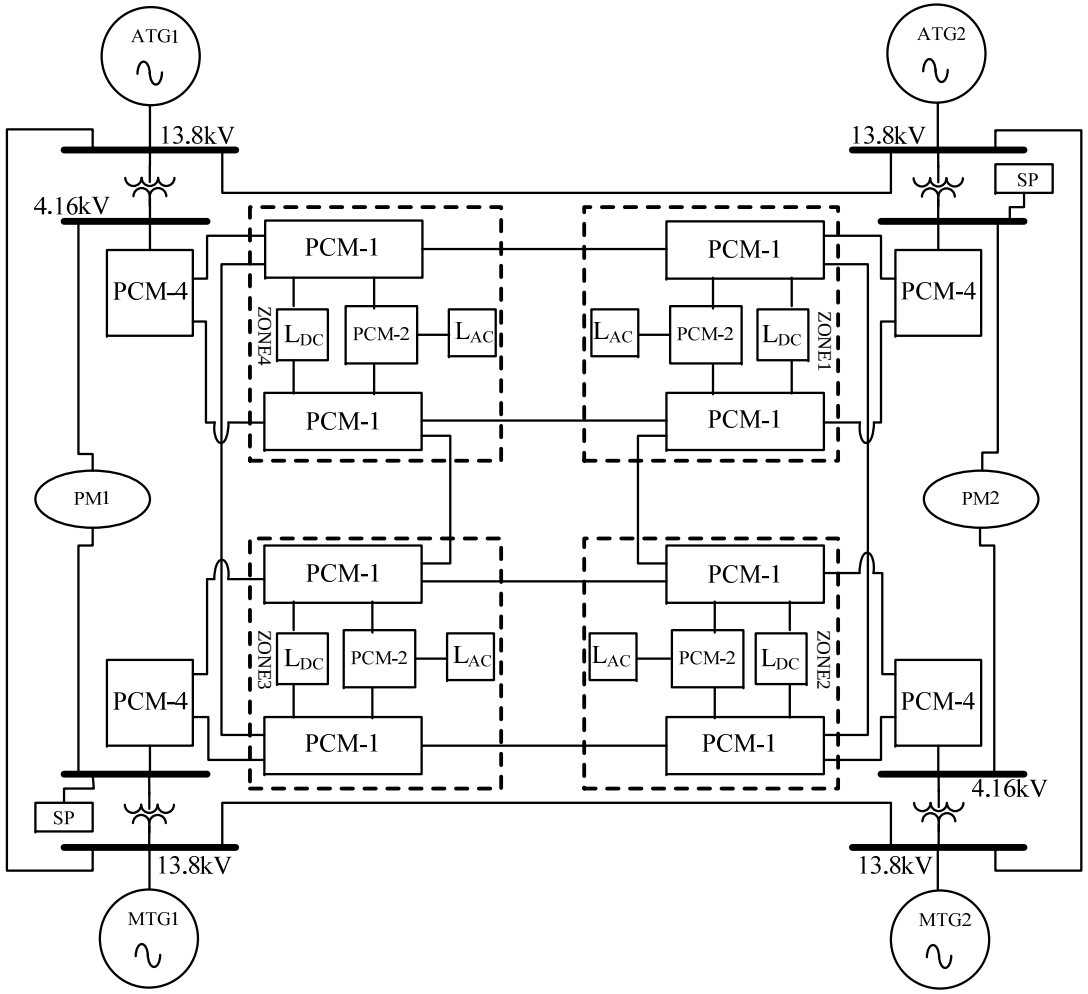

Fig. 3.3. Notional NGIPS Shipboard Power System Architecture

3.4 PROBLEM STATEMENT

In order to analyze the potential communication capability of the shipboard IPS system of the NGIPS, for use as an automation communication channel that will enable remote monitoring of various ship components from a central location, it is necessary to understand the communication characteristics of the various components such as circuit breakers, bus transfers, transformers, switches, power converters, cables, and other IPS components. Other factors such as ship reconfiguration, inherent noise in the ship power system and electromagnetic interference issues also need to be considered.

An analytical model for characterizing the BPL/PLC response of the NGIPS class power system will require and the development of a BPL/PLC channel response analytical model for each of the above mentioned SPS network components. Where it is widely known that low-power high-frequency signals like those used in BPL/PLC systems are severely attenuated by transformers [9, 10], the effect of passing BPL/PLC signals through other SPS components have not been studied and clearly established. The scope of this research will be to analytically model the data capacity characteristics of various ship board (marine) power cable sizes and types that may be used in the NGIPS based on the voltage levels and ampacity in the different segments of the notional NGIPS topology considered.

3.5 SUMMARY

A general description of the automation system in U.S Navy ships was discussed in this section. Emphasizing the importance of the communication system in the ship automation system, a brief description of the importance of the automation of ship systems indicating the role of the communication network was presented. The notional NGIPS class SPS topology, showing the various components of the SPS, component connection and voltage levels, was also presented. Finally, the actual work addressed by in this research was specified. In the next section, the approach used in developing the analytical model for determining the BPL/PLC channel characteristics of the ship power cables of the NGIPS will be discussed.

4. SOLUTION METHODOLOGY

4.1 INTRODUCTION

In order to develop an analytical model for characterizing the BPL/PLC channel characteristics of the shipboard power cables, a BPL/PLC channel model for indoor and office power lines, based on the multiconductor transmission line theory, was adapted. A multiconductor transmission line is typically defined as a transmission line with $(n+1)$ parallel conductors that serve to transmit electrical signals between two or more points [23], where *n* is typically greater than or equal to one. In this section, the approach taken to develop the analytical model for the BPL/PLC analysis of shipboard power cables is discussed. Various transmission line theories, including the established Two-port network representation of a Two-conductor transmission line, that were applied in the development of the BPL/PLC model are presented.

4.2 SOLUTION APPROACH

Ship power system topologies are usually of a Three-phase floating ground configuration [3]. Particularly, U.S. Navy ship power systems use an ungrounded Three-phase delta configuration. This configuration has inherent fault tolerance, as a power system based on this configuration will remain in operation even in the event of a single-phase-to-hull fault [24]. The ungrounded Three-phase delta configuration of the SPS uses Three-phase cables with no neutral conductor. The presence of three conductors inherently makes the ship transmission lines a Multiconductor Transmission Line

(MTL)[23]. This work adapted an indoor power-line model based on the MTL theory to develop an analytical model to examine the channel response characteristics of the shipboard power system transmission lines and estimated the channel throughput capacity of the transmission lines using a “water-filling” communication technique.

The solution approach used is shown in the flow chart in Fig. 4.1. The three-conductor, in-door transmission line model in [13], which was developed for residential and office power systems, the majority of which are comprised of grounded single-phase three-wire topologies, was modified to match the SPS topology. The model also factored in certain connection practices such as bonding, which is the connection of the ground and return wire via a shunt conductance within the service panel, which is common in residential systems. The modified model allowed the SPS BPL channel to be modeled as a Two-conductor transmission line. A three-step approach for modeling the BPL channel of the NGIPS power cables as a Two-conductor transmission line was used. The primary line parameter values (R, L, C, and G) are first calculated and used to obtain the characteristic impedance Z_c and propagation constant γ. These parameters are used to calculate the transfer function of the NGIPS channel using the Two-port network model of the power lines. The frequency response of the channel is computed from the transfer function. Finally, using the obtained frequency response, a “water-filling” communication technique is used to estimate the data throughput capacity of the power line channel.

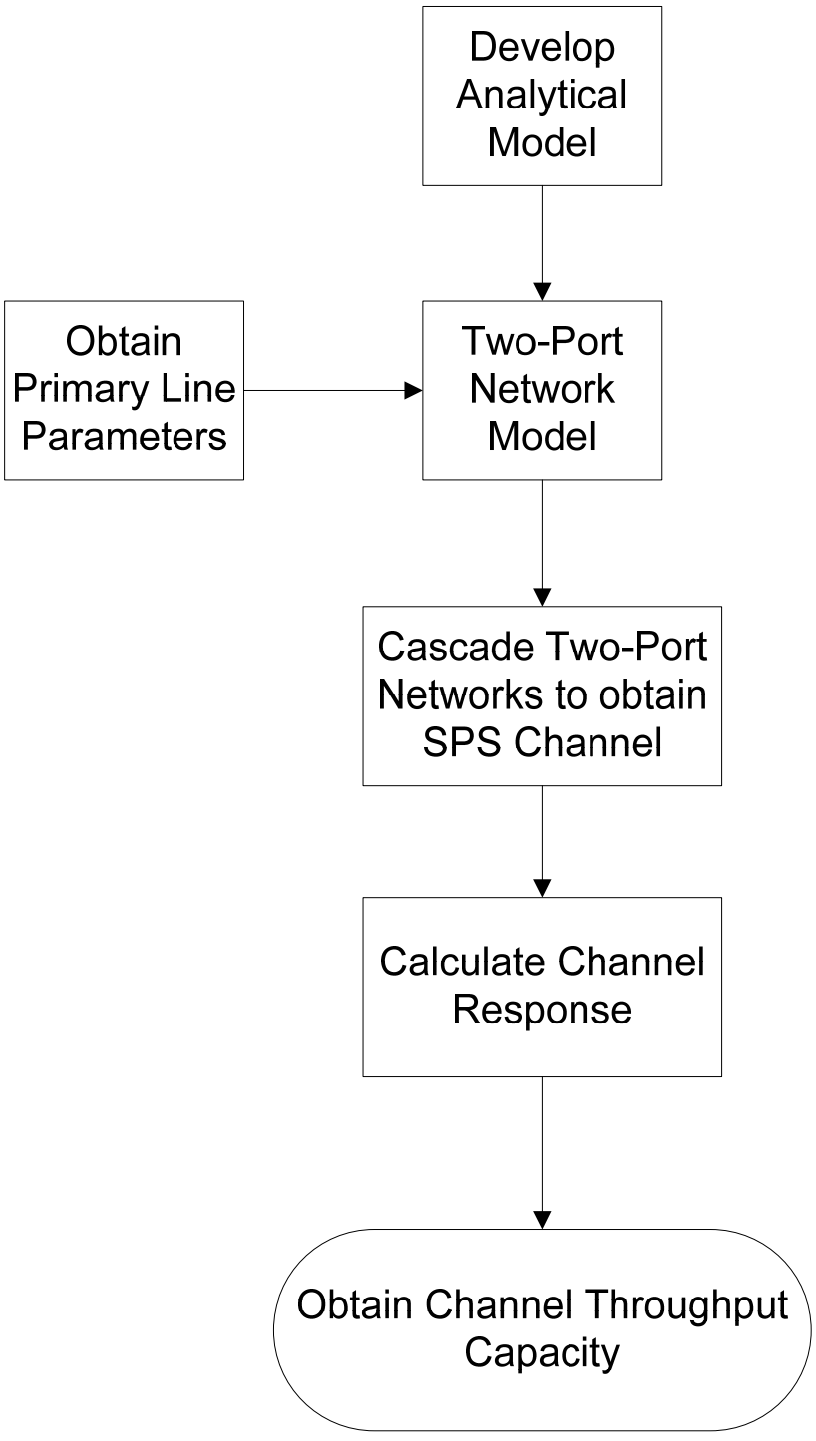

Fig. 4.1. Solution Methodology Flow Chart

4.3 ANALYTICAL MODEL

The analytical model adapted in this work is based on the multiconductor transmission line (MTL) theory [13, 25, 26]. The development of the model from the MTL theory using transverse electromagnetic wave approximations will be described in this section. The SPS BPL channel model using this approach will then be developed.

4.3.1 MTL Analysis of SPS Transmission Lines

Application of BPL in ships requires the BPL signal to be coupled to only two of the three SPS conductors [3], as illustrated in Fig. 4.2. Based on the transverse electromagnetic approximation, if two of the conductors are excited (V_A,V_B), and the third conductor is at a potential V_C, the three-conductor cable will support three spatial modes (differential mode, pair mode and common mode) propagating in the forward and backward directions[13]. Using the MTL theory[27], the voltages and current equations of the three-conductor transmission lines can be decoupled via transformation to the corresponding modal voltages and currents. Fig. 4.3 shows the equivalent circuit which describes the deconvolution of the propagating modes for a finite section of a power cable [25]. If the forward propagating mode voltages and currents are defined as $\mathbf{V}_1^+ = \left(V_{dif}^+, V_{pr}^+, V_{cm}^+\right)$ and $\mathbf{I}_1^+ = \left(I_{dif}^+, I_{pr}^+, I_{cm}^+\right)$ respectively, and the negative propagating mode signals are defined as $\mathbf{V}_1^- = \left(V_{dif}^-, V_{pr}^-, V_{cm}^-\right)$ and $\mathbf{I}_1^- = \left(I_{dif}^-, I_{pr}^-, I_{cm}^-\right)$, the relationship between the line excitation voltages and currents and the three propagating modes can be described in equations (1) and (2). From Fig. 4.3, it can be seen that an incident

differential signal on the left, characterized by V_{dif} and I_{dif} appears on the far right end as a dependent voltage $(I_{dif}Z_{dif}+V_{dif})e^{-\gamma_{dif}(s)x}$ where $\gamma_{dif(s)}$ is the complex propagation constant for the differential spatial mode and x is the position along the transmission line [13].

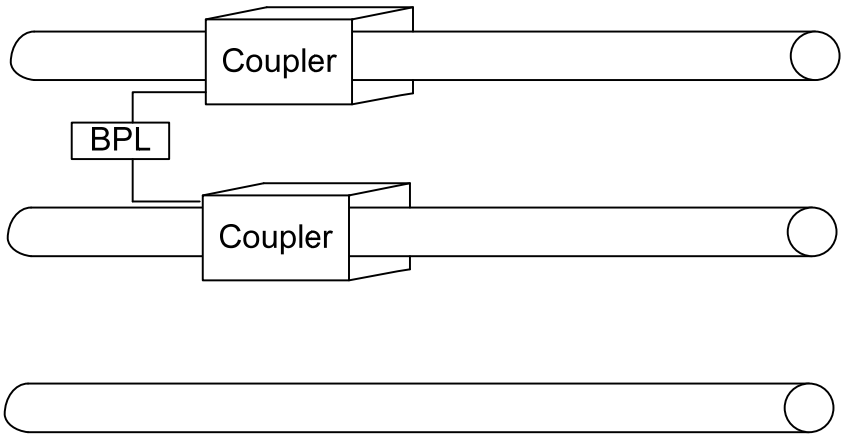

Fig. 4.2. Signal Coupling Scheme [3]

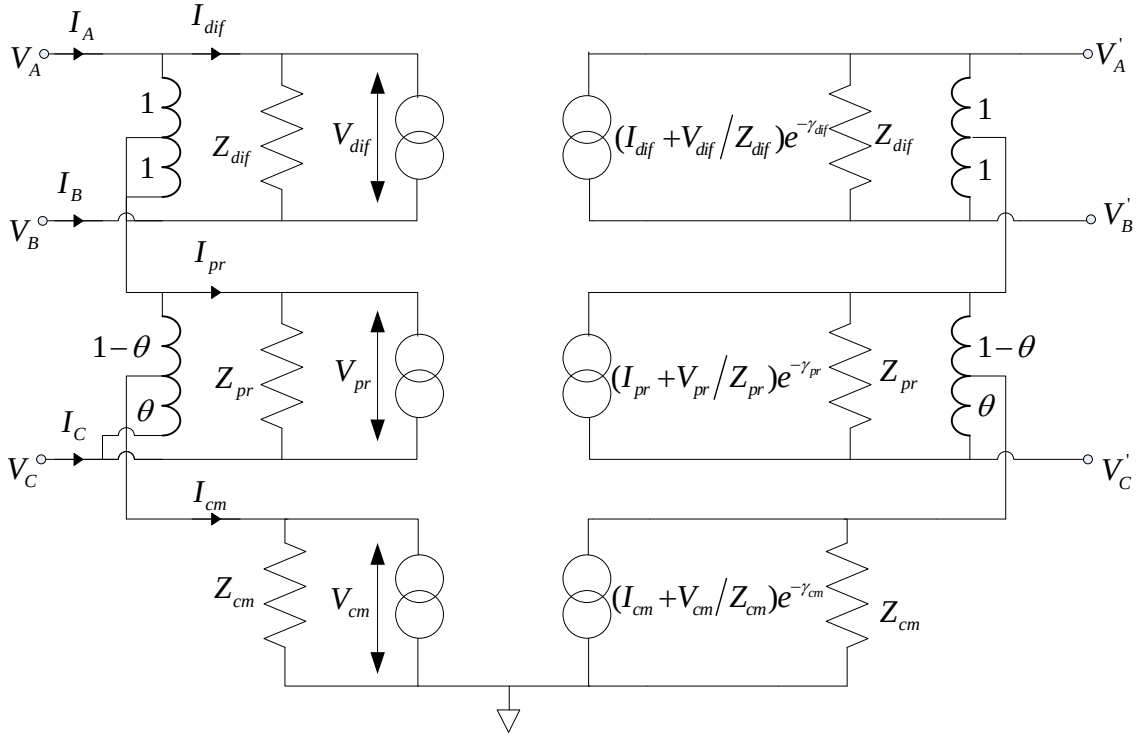

Fig. 4.3. Equivalent Circuit Representing the Three Dominant Modes [25]

$$\mathbf{V}_1 \equiv \mathbf{V}_1^+ + \mathbf{V}_1^- \equiv \begin{bmatrix} V_{dif}^+ \\ V_{pr}^+ \\ V_{cm}^+ \end{bmatrix} + \begin{bmatrix} V_{dif}^- \\ V_{pr}^- \\ V_{cm}^- \end{bmatrix} = \begin{bmatrix} 1 & -1 & 0 \\ 1/2 & 1/2 & -1 \\ 1/2\,\theta & 1/2\,\theta & 1-\theta \end{bmatrix} \begin{bmatrix} V_A \\ V_B \\ V_C \end{bmatrix} \equiv \mathbf{A}\mathbf{V}_P \tag{1}$$

$$\mathbf{I}_1 \equiv \mathbf{I}_1^+ - \mathbf{I}_1^- \equiv \begin{bmatrix} I_{dif}^+ \\ I_{pr}^+ \\ I_{cm}^+ \end{bmatrix} - \begin{bmatrix} I_{dif}^- \\ I_{pr}^- \\ I_{cm}^- \end{bmatrix} = \begin{bmatrix} 1/2 & -1/2 & 0 \\ 1-\theta & 1-\theta & -\theta \\ 1 & 1 & 1 \end{bmatrix} \begin{bmatrix} I_A \\ I_B \\ I_C \end{bmatrix} \equiv \mathbf{B}\mathbf{I}_P \tag{2}$$

Where $\mathbf{V}_P = (V_A, V_B, V_C)$ and $\mathbf{I}_P = (I_A, I_B, I_C)$ are the voltages and currents on the three conductors, respectively. **A** and **B** are transformation matrices and the factor θ

describes the shielding due to the third conductor, where $\theta \approx 0.15$ for NM type cable[13]. It should be noted that:

$$\mathbf{B}^{-1} = \mathbf{A}^{T}, \mathbf{A}^{-1} = \mathbf{B}^{T} \tag{3}$$

The propagating voltages $\mathbf{V}_1^+$ and $\mathbf{V}_1^-$ are related to the corresponding currents $\mathbf{I}_1^+$ and $\mathbf{I}_1^-$ by a diagonal matrix $\mathbf{Z}_0$ of characteristic impedances as shown in equations (4) and (5).

$$\mathbf{V}_1^+ \equiv \begin{bmatrix} V_{dif}^+ \\ V_{pr}^+ \\ V_{cm}^+ \end{bmatrix} = \begin{bmatrix} Z_{dif} & 0 & 0 \\ 0 & Z_{pr} & 0 \\ 0 & 0 & Z_{cm} \end{bmatrix} \begin{bmatrix} I_{dif}^+ \\ I_{pr}^+ \\ I_{cm}^+ \end{bmatrix} \equiv \mathbf{Z}_0 \mathbf{I}_1^+ \tag{4}$$

$$\mathbf{V}_1^- \equiv \begin{bmatrix} V_{dif}^- \\ V_{pr}^- \\ V_{cm}^- \end{bmatrix} = \begin{bmatrix} Z_{dif} & 0 & 0 \\ 0 & Z_{pr} & 0 \\ 0 & 0 & Z_{cm} \end{bmatrix} \begin{bmatrix} I_{dif}^- \\ I_{pr}^- \\ I_{cm}^- \end{bmatrix} \equiv -\mathbf{Z}_0 \mathbf{I}_1^- \tag{5}$$

4.3.2 Channel Model

Applying the MTL analysis for modeling the BPL channel of the shipboard power system cables, the cable length is first consider to be semi-infinite to facilitate the calculation of the cable's impedance. Application of an input voltage signal $\mathbf{V}_p$ at one end of the cable will excite only forward propagating modal voltages [13], which implies that $\mathbf{V}_1^- = 0$ and $\mathbf{I}_1^- = 0$. Substituting $\mathbf{V}_1^- = 0$ into (1) gives

$$\mathbf{V}_1^+ = \mathbf{A}\mathbf{V}_P \tag{6}$$

Recalling (4) and (5),

$$\mathbf{Z}_0\mathbf{I}_1^+ = \mathbf{A}\mathbf{V}_P \tag{7}$$

$$\mathbf{Z}_0\mathbf{B}\mathbf{I}_P = \mathbf{A}\mathbf{V}_P \tag{8}$$

$$\mathbf{V}_P = \mathbf{A}^{-1}\mathbf{Z}_0\mathbf{B}\mathbf{I}_P = \mathbf{Z}_P^{\infty}\mathbf{I}_P \tag{9}$$

Where $\mathbf{Z}_P^{\infty}$ is the terminal impedance observed when looking into the semi-infinite long cable and $\mathbf{Y}_P^{\infty}$ is the corresponding conductance.

$$\mathbf{Z}_P^{\infty} = \mathbf{A}^{-1}\mathbf{Z}_0\mathbf{B} = \mathbf{B}^T\mathbf{Z}_0\mathbf{B} \tag{10}$$

$$\mathbf{Y}_P^{\infty} = (\mathbf{Z}_P^{\infty})^{-1} = \mathbf{A}^T\mathbf{Z}_0^{-}\mathbf{A} \tag{11}$$

Now consider that a purely differential incident traveling wave $\mathbf{I}_1^+ = (I_{dif}^+, 0, 0)$ is applied to the cable and the cable is terminated in an impedance matrix $\mathbf{Z}_{term}$, the reflected wave $\mathbf{I}_1^-$ may contain additional propagating mode components[13]. The relationship between the forward and backward traveling waves may be obtained by expressing the voltages and currents in the cable in terms of propagating modes.

$$\mathbf{V}_P = \mathbf{Z}_{term}\mathbf{I}_P \tag{12}$$

$$\mathbf{I}_1^+ - \mathbf{I}_1^- = \mathbf{B}\mathbf{I}_P \tag{13}$$

$$\mathbf{V}_1^+ + \mathbf{V}_1^- = \mathbf{A}\mathbf{V}_P \tag{14}$$

Solving for the reflected current $\mathbf{I}_1^-$, recall that

$$\mathbf{V}_1^+ = \mathbf{Z}_0\mathbf{I}_1^+;\ \mathbf{V}_1^- = \mathbf{Z}_0\mathbf{I}_1^-;\ \mathbf{I}_P = \mathbf{B}^{-1}(\mathbf{I}_1^+ - \mathbf{I}_1^-) = \mathbf{A}^T(\mathbf{I}_1^+ - \mathbf{I}_1^-)$$

Therefore,

$$\mathbf{Z}_0\mathbf{I}_1^+ + \mathbf{Z}_0\mathbf{I}_1^- = \mathbf{A}\mathbf{Z}_{term}\mathbf{A}^T(\mathbf{I}_1^+ - \mathbf{I}_1^-) \tag{15}$$

$$\mathbf{Z}_0\mathbf{I}_1^- + \mathbf{A}\mathbf{Z}_{term}\mathbf{A}^T\mathbf{I}_1^- = \mathbf{A}\mathbf{Z}_{term}\mathbf{A}^T\mathbf{I}_1^+ - \mathbf{Z}_0\mathbf{I}_1^+ \tag{16}$$

$$(\mathbf{Z}_0 + \mathbf{A}\mathbf{Z}_{term}\mathbf{A}^T)\mathbf{I}_1^- = (\mathbf{A}\mathbf{Z}_{term}\mathbf{A}^T - \mathbf{Z}_0)\mathbf{I}_1^+ \tag{17}$$

Similarly;

$$\mathbf{I}_1^- = \mathbf{V}_1^-\mathbf{Z}_0^{-1};\ \mathbf{I}_1^+ = \mathbf{V}_1^+\mathbf{Z}_0^{-1}$$

$$\mathbf{V}_1^+\mathbf{Z}_0^{-1} - \mathbf{V}_1^-\mathbf{Z}_0^{-1} = \mathbf{B}\mathbf{Z}_{term}^{-1}\mathbf{V}_P \tag{18}$$

But

$$\mathbf{V}_P = \mathbf{A}^{-1}(\mathbf{V}_1^+ + \mathbf{V}_1^-) = \mathbf{B}^T(\mathbf{V}_1^+ + \mathbf{V}_1^-) \tag{19}$$

$$\mathbf{V}_1^+\mathbf{Z}_0^{-1} - \mathbf{V}_1^-\mathbf{Z}_0^{-1} = \mathbf{B}\mathbf{Z}_{term}^{-1}\mathbf{B}^T(\mathbf{V}_1^+ + \mathbf{V}_1^-) \tag{20}$$

$$\mathbf{V}_1^+\mathbf{Z}_0^{-1} - \mathbf{V}_1^-\mathbf{Z}_0^{-1} = \mathbf{B}\mathbf{Z}_{term}^{-1}\mathbf{B}^T\mathbf{V}_1^+ + \mathbf{B}\mathbf{Z}_{term}^{-1}\mathbf{B}^T\mathbf{V}_1^- \tag{21}$$

$$\mathbf{V}_1^+\mathbf{Z}_0^{-1} - \mathbf{B}\mathbf{Z}_{term}^{-1}\mathbf{B}^T\mathbf{V}_1^+ = \mathbf{V}_1^-\mathbf{Z}_0^{-1} + \mathbf{B}\mathbf{Z}_{term}^{-1}\mathbf{B}^T\mathbf{V}_1^- \tag{22}$$

$$(\mathbf{Z}_0^{-1} - \mathbf{B}\mathbf{Z}_{term}^{-1}\mathbf{B}^T)\mathbf{V}_1^+ = (\mathbf{Z}_0^{-1} + \mathbf{B}\mathbf{Z}_{term}^{-1}\mathbf{B}^T)\mathbf{V}_1^- \tag{23}$$

If $\boldsymbol{\rho}_I$ and $\boldsymbol{\rho}_V$ are defined as the current and voltage reflection coefficient matrices, the backward traveling waves or reflected waves are related to the incident or forward traveling waves by (24) and (25) [13].

$$\mathbf{I}_1^- = \boldsymbol{\rho}_I\mathbf{I}_1^+ \tag{24}$$

$$\mathbf{V}_1^- = \boldsymbol{\rho}_V\mathbf{V}_1^+ \tag{25}$$

Using (4) and (5), the relationship between the two reflection coefficient matrices can be obtained as in (26) to (29)

$$-\mathbf{Z}_0\boldsymbol{\rho}_I\mathbf{I}_1^+ = \boldsymbol{\rho}_V\mathbf{Z}_0\mathbf{I}_1^+ \tag{26}$$

$$\mathbf{V}_1^- = \boldsymbol{\rho}_V\mathbf{Z}_0\mathbf{I}_1^+ \tag{27}$$

$$-\mathbf{Z}_0\mathbf{I}_1^- = \boldsymbol{\rho}_V\mathbf{Z}_0\mathbf{I}_1^+ \tag{28}$$

$$\boldsymbol{\rho}_V = -\mathbf{Z}_0\boldsymbol{\rho}_I\mathbf{Z}_0^{-1} \tag{29}$$

By comparing (17) and (23) to (24) and (25), the reflection coefficients can be expressed as in (30) and (31). Note that reflections are suppressed when $\boldsymbol{\rho}_V = \boldsymbol{\rho}_I = 0$ [13].

$$\boldsymbol{\rho}_V = (\mathbf{Z}_0^{-1} + \mathbf{B}\mathbf{Z}_{term}^{-1}\mathbf{B}^T)^{-1}(\mathbf{Z}_0^{-1} - \mathbf{B}\mathbf{Z}_{term}^{-1}\mathbf{B}^T) \tag{30}$$

$$\boldsymbol{\rho}_I = (\mathbf{Z}_0 + \mathbf{A}\mathbf{Z}_{term}\mathbf{A}^T)^{-1}(\mathbf{Z}_0 - \mathbf{A}\mathbf{Z}_{term}\mathbf{A}^T) \tag{31}$$

In the general case that a shunt conductance is placed between the conductors of a three conductor transmission line, as shown in Fig. 4.4, the mode coupling produced by these conductance Z_{AB}, Z_{AC} and Z_{BC} can be examined[26]. The conductance matrix $\mathbf{Y}_{sh}$ for this case is given in (32). The effective termination seen by the excited cable is $\mathbf{Y}_{term}$.

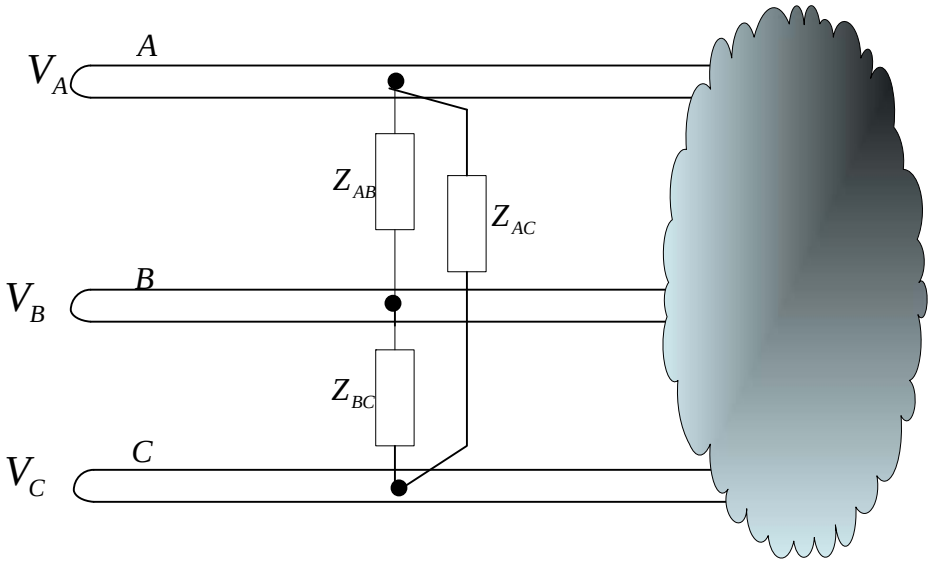

Fig. 4.4. Model for Examining Mode Coupling Due to Shunt Conductance between the Conductors

$$\mathbf{Y}_{sh} = \begin{bmatrix} 1/Z_{AC} + 1/Z_{AB} & -1/Z_{AB} & -1/Z_{AC} \\ -1/Z_{AB} & 1/Z_{BC} + 1/Z_{AB} & -1/Z_{BC} \\ -1/Z_{AC} & -1/Z_{BC} & 1/Z_{BC} + 1/Z_{AC} \end{bmatrix} \tag{32}$$

$$\mathbf{Y}_{term} = (\mathbf{Z}_{term})^{-1} = \mathbf{A}^T \mathbf{Z}_0^{-1} \mathbf{A} + \mathbf{Y}_{sh} \tag{33}$$

Therefore,

$$\boldsymbol{\rho}_V = -(2\mathbf{A}^T \mathbf{Z}_0^{-1} + \mathbf{Y}_{sh} \mathbf{B}^T)^{-1} \mathbf{Y}_{sh} \mathbf{B}^T \tag{34}$$

For this work, the application of a purely differential incident wave $\mathbf{V}_1^+ = (V_{dif}^+, 0, 0)$, BPL signal coupled onto conductors A and B in Fig. 4.4 is considered. During normal operation, only the load impedance of the receiver, represented by Z_{AB} is connected between the two conductors. Placing only Z_{AB} in the conductance matrix $\mathbf{Y}_{sh}$

and setting $Z_{BC} = Z_{AC} = \infty$ as shown in Fig. 4.5, the resultant conductance matrix can be expressed as in (35). Substituting this conductance matrix into (34) will yield (36) to (38).

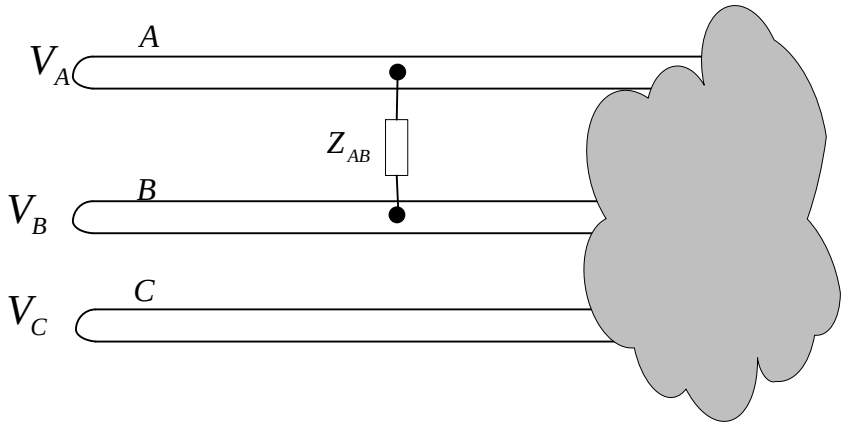

Fig. 4.5. Model for Examining Mode Coupling Due to Shunt Conductance across Conductors A and B

$$\mathbf{Y}_{sh,AB} = \begin{bmatrix} \frac{1}{Z_{AB}} & \frac{-1}{Z_{AB}} & 0 \\ \frac{-1}{Z_{AB}} & \frac{1}{Z_{AB}} & 0 \\ 0 & 0 & 0 \end{bmatrix} \tag{35}$$

$$\boldsymbol{\rho}_V = \begin{bmatrix} \dfrac{-Z_{dif}}{2R_L + Z_{dif}} & 0 & 0 \\ 0 & 0 & 0 \\ 0 & 0 & 0 \end{bmatrix} \tag{36}$$

$$V_{dif}^{-} \equiv \boldsymbol{\rho}_{V,dif}^{(L)} V_{dif}^{+} = -\frac{Z_{dif}}{2R_L + Z_{dif}} V_{dif}^{+} \tag{37}$$

$$V_{pr}^{-} = V_{cm}^{-} = 0 \tag{38}$$

Thus, there is no coupling between the spatial modes. Futhermore, due to decoupling the MTL equations, the resultant differential mode can be modeled as a simple Two-conductor transmission line [13].

4.4 PRIMARY LINE CHARACTERISTICS

Transmission lines are characterized by their characteristic impedance (Z_c) and their propagation constant (γ). The standard equations for calculating Z_c and γ are given in (39) and (40) respectively. Where R is the per-unit line resistance, L is the per-unit-inductance, C is the per-unit-capacitance, G is the per-unit line conductance, and $\omega = 2\pi f$. It should be noted that these basic line parameters (R, L, C, G) are frequency dependent and can be obtained from expressions, given in the following sub-sections, which use the ship cable specifications.

$$Z_C = \sqrt{\frac{z}{y}} = \sqrt{\frac{R + j\omega L}{G + j\omega C}} \tag{39}$$

$$\gamma = \sqrt{zy} = \sqrt{(R + j\omega L)(G + j\omega C)} \tag{40}$$

4.4.1 Per-Unit-Length Resistance

The transmission line cables used in a ship power system have a less than perfect conductivity ($\sigma < 100\%$), as such the current flow internal to the conductors produces a per-unit length resistance r [28]. As illustrated in Fig. 4.6, with a direct current (dc), ($f = 0$), excitation, the current is uniformly distributed over the cross section of a solid conductor. However, as the frequency of excitation increases, the current tends to cluster closer to the outside of the conductor. This is called *skin effect* and the thickness of the region of the conductor occupied by the current is known as *skin depth* δ [23, 28]. The frequency dependent per-unit-length expression used in this work is given in (41).

$$R(f) = \frac{1}{2\pi r_w \sigma \delta} = \frac{1}{2r_w}\sqrt{\frac{\mu}{\pi\sigma}}\sqrt{f} \quad \left(\Omega/m\right) \tag{41}$$

$$\delta = \sqrt{\frac{1}{\pi f \mu \sigma}} \tag{42}$$

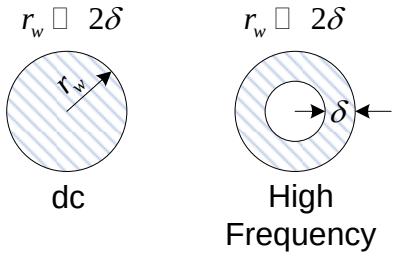

Fig. 4.6. Current Distribution in Conductor with Frequency Level

4.4.2 Per-Unit-Length Inductance

The per-unit-length inductance of a Two-conductor transmission line, shown in fig , includes the self/internal inductance l_i of each conductor, and the mutual/external inductance l_e between the two conductors. The total per-unit-length inductance of a Two-conductor transmission line is given in (43) to (46) [28].

$$l = 2l_i + l_e \tag{43}$$

$$l_i = \frac{1}{4\pi r_w}\sqrt{\frac{\mu}{\pi\sigma}}\frac{1}{\sqrt{f}} \quad \left(H/m\right) \tag{44}$$

$$l_e = \frac{\mu}{\pi}\ln\left(\frac{s}{r_w}\right) \quad \left(H/m\right) \tag{45}$$

$$L(f) = \left(\frac{2}{4\pi r_w}\sqrt{\frac{\mu}{\pi\sigma}} * \frac{1}{\sqrt{f}} + \frac{\mu}{\pi}\ln(\frac{s}{r_w})\right) \left(H/m\right) \tag{46}$$

4.4.3 Per-Unit-Length Capacitance

Based on the TEM mode of propagation theory, a relationship exists between the per-unit-length external inductance l_e, capacitance C, and the conductance G, given that the conductors are in a homogeneous medium characterized by σ, μ and ε [28]. This relationship is expressed in (47) and (48). Therefore, the per-unit-length capacitance of the Two-conductor transmission line is expressed in (49).

$$l_e g = \mu\sigma \tag{47}$$

$$l_e c = \mu\varepsilon \tag{48}$$

$$C = \frac{\pi\varepsilon}{\ln\left(s/r_w\right)} \quad \left(F/m\right) \tag{49}$$

4.4.4 Per-Unit-Length Conductance

From the relationship established in section 4.4.3, the per-unit-length conductance a Two-conductor transmission line is given in

$$G = \frac{\pi\sigma}{\ln\left(s/r_w\right)} \quad \left(\square/m\right) \tag{50}$$

4.5 TWO-PORT NETWORK MODEL OF TWO-CONDUCTOR TRANSMISSION LINE

A Two-port network is a linear electrical circuit with two pairs of terminals, such that the voltages and currents at one port (pair of terminals) may be expressed as linear combinations of the voltages and currents at the other terminal. The Two-port network model of a Two-conductor transmission line will be developed in this section. Using Fig. 4.7 below, to illustrate the basic two cable transmission line configuration of length Δx, where $i(x)$ and $V(x)$ represent the current and voltage at the receiving end of the transmission line and $i(x+\Delta x)$, $V(x+\Delta x)$ represent the current and voltage at the sending end of the transmission line. The channel characteristics of the SPS power lines were investigated over a frequency range of 1-30MHz. At these frequencies, the distributed parameter line model must be used because the length of the SPS cables are much greater than a tenth of the signal wavelength [23].

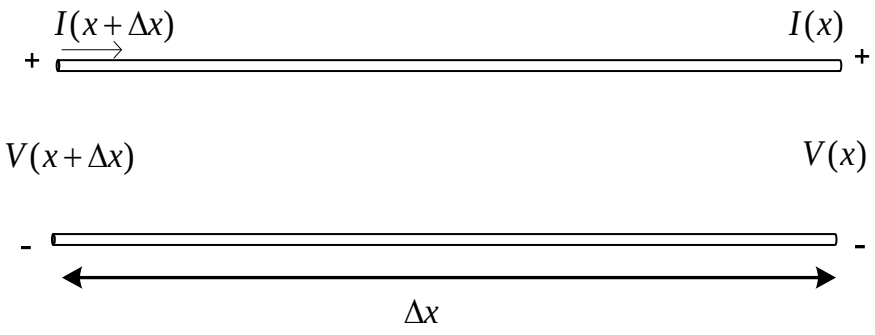

Fig. 4.7. Simple Two-cable Transmission Line

Using the distributed parameter line theory, the transmission line configuration in Fig. 4.7 above can be modeled as shown in Fig. 4.8 below. In the distributed parameter model, the unit line constants (resistance (R), inductance (L), Conductance (G) and capacitance (C)) are considered to be uniformly distributed along the transmission line. Where,

$$z = R + j\omega L \tag{51}$$

$$y = G + j\omega C \tag{52}$$

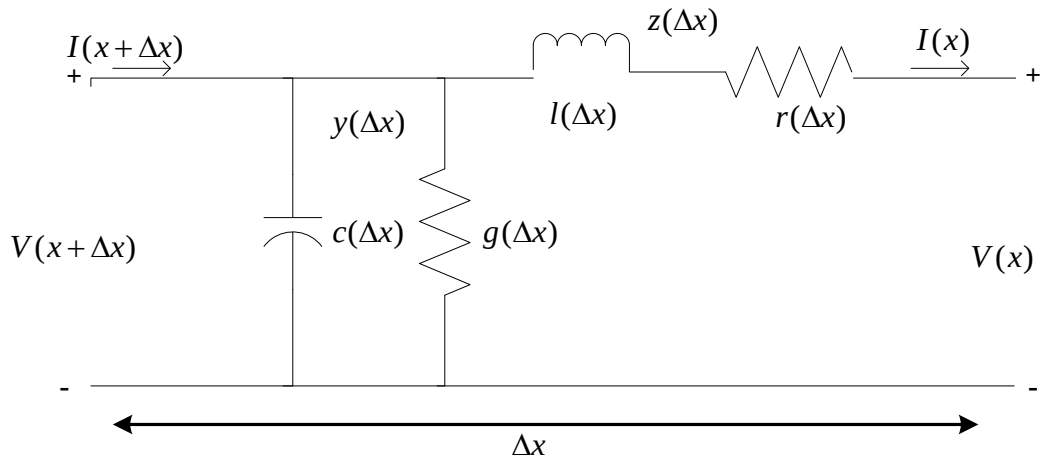

Fig. 4.8. Distributed Parameter Transmission Line

The Two-conductor Two-port network model can be obtained from the distributed parameter model using the Kirchoff's current and voltage laws. The derivation of the Two-port network model is given in the expressions in (53) thru (69). From Fig. 4.8, writing a KVL equation will give (53) which can be rearranged to the form shown in (54). Similarly, from KCL, the distributed parameter model yields (55) which when rearranged can be expressed as (56). Combining (54) and (56) results in (57) which gives (58).

$$V(x+\Delta x) = V(x) + (z\Delta x)I(x) \tag{53}$$

$$\frac{V(x+\Delta x) - V(x)}{\Delta x} = zI(x) \equiv \frac{dV(x)}{dx} = zI(x) \tag{54}$$

$$I(x+\Delta x) = I(x) + (y\Delta x)V(x) \tag{55}$$

$$\frac{I(x+\Delta x)-I(x)}{\Delta x}=yV(x)\equiv\frac{dI(x)}{dx}=yV(x) \tag{56}$$

$$\frac{d^2V(x)}{dx^2}=z\frac{dI(x)}{dx}=zyV(x) \tag{57}$$

$$\frac{d^2V(x)}{dx^2}-zyV(x)=0 \tag{58}$$

Equation (58) can be solved by inspection using $V(x)=A_1e^{\gamma x}+A_2e^{-\gamma x}$ where $\gamma=\sqrt{zy}$. Differentiating $V(x)=A_1e^{\gamma x}+A_2e^{-\gamma x}$ will yield (59) and the expression for $I\left(x\right)$ is given in (60).

$$\frac{dV(x)}{dx}=\gamma A_1e^{\gamma x}-\gamma A_2e^{-\gamma x}=zI(x) \tag{59}$$

$$I(x)=\frac{A_1e^{\gamma x}-A_2e^{-\gamma x}}{z/\gamma}\equiv\frac{A_1e^{\gamma x}-A_2e^{-\gamma x}}{z/\sqrt{zy}} \tag{60}$$

Where, $z/\gamma=z/\sqrt{zy}=\sqrt{z/y}=z_c$. $A_1=\frac{V_R+z_cI_R}{2}$ and $A_2=\frac{V_R-z_cI_R}{2}$ giving that V_R and I_R are the receiving end voltage and current. Substituting A_1 and A_2 into $V(x)$ and $I(x)$ gives (61) and (62) which can be rearranged and expressed in the form shown in (63) and (64). Equations (63) and (64) can be re-written, using hyperbolic trigonometric functions given in (65) and (66), as shown in (67) and (68).

$$V(x)=\left(\frac{V_R+z_cI_R}{2}\right)e^{\gamma x}+\left(\frac{V_R-z_cI_R}{2}\right)e^{-\gamma x} \tag{61}$$

$$I(x) = \left(\frac{V_R + z_c I_R}{2 z_c} \right) e^{\gamma x} - \left(\frac{V_R - z_c I_R}{2 z_c} \right) e^{-\gamma x} \tag{62}$$

$$V(x) = \left(\frac{e^{\gamma x} + e^{-\gamma x}}{2} \right) V_R + z_c \left(\frac{e^{\gamma x} - e^{-\gamma x}}{2} \right) I_R \tag{63}$$

$$I(x) = \frac{1}{z_c} \left(\frac{e^{\gamma x} - e^{-\gamma x}}{2} \right) V_R + \left(\frac{e^{\gamma x} + e^{-\gamma x}}{2} \right) I_R \tag{64}$$

$$\left(\frac{e^{\gamma x} + e^{-\gamma x}}{2} \right) = \cosh(\gamma x) \tag{65}$$

$$\left(\frac{e^{\gamma x} - e^{-\gamma x}}{2} \right) = \sinh(\gamma x) \tag{66}$$

$$V(x) = \cosh(\gamma x) V_R + z_c \sinh(\gamma x) I_R \tag{67}$$

$$I(x) = \frac{1}{z_c} \sinh(\gamma x) V_R + \cosh(\gamma x) I_R \tag{68}$$

The expressions in (67) and (68) can be written in matrix form in (69), where $V(x)$ and $I(x)$ are the voltage and current at location *x* along the transmission line. $A(x) = D(x) = \cosh(\gamma x)$, $B(x) = z_c \sinh(\gamma x)$ (Ω) and $C(x) = 1/z_c \sinh(\gamma x)$ (s) . A general result of the transmission line theory is that every uniform transmission line can be modeled as a Two-port network (2PN). Representing the transmission line configuration as a Two-port network of the form in Fig. 4.9 below, the relationship between the sending and receiving end quantities can be written as in (70).

$$\begin{bmatrix} V(x) \\ I(x) \end{bmatrix} = \begin{bmatrix} A(x) & B(x) \\ C(x) & D(x) \end{bmatrix} \begin{bmatrix} V_R \\ I_R \end{bmatrix} \tag{69}$$

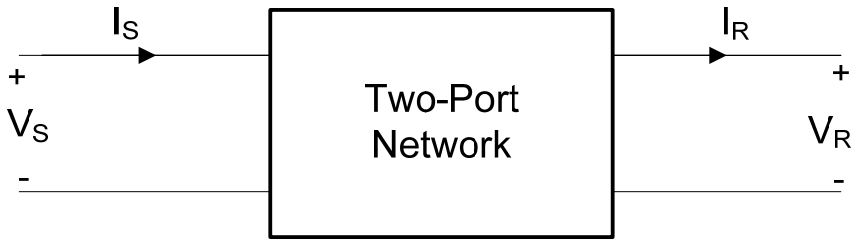

Fig. 4.9. Basic Two-port Network Model

$$\begin{bmatrix} V_s \\ I_s \end{bmatrix} = \begin{bmatrix} A & B \\ C & D \end{bmatrix} \begin{bmatrix} V_R \\ I_R \end{bmatrix} \tag{70}$$

$$V_s = AV_R + BI_R \tag{71}$$

$$I_s = CV_R + DI_R \tag{72}$$

4.6 FREQUENCY RESPONSE OF THE CHANNEL

Applying the Two-port network model that was derived in the previous section, the channel frequency response of the SPS transmission lines to the applied differential wave BPL signal excitation can be examined. The differential excitation signal V_S is coupled to the line at the left port with input impedance Z_s, and the output signal V_R is received at the load, $Z_{L,}$ end. Representing the transmission line configuration as a Two-port network of the form in Fig. 4.10, the relationship between the sending and receiving

end is shown in (70) becomes (73) This is rewritten in (74) with respect to the receiving end. In (75) and (76), the relationship between the input and output signals V_S and V_R to the two port parameters is shown. Finally, the transfer function, $H(f)$, of the cable channel of length l is obtained in (77). In this work, the transfer function is plotted over a frequency range of 1 – 30 MHz and converted into decibels (dB) by the expression in (78).

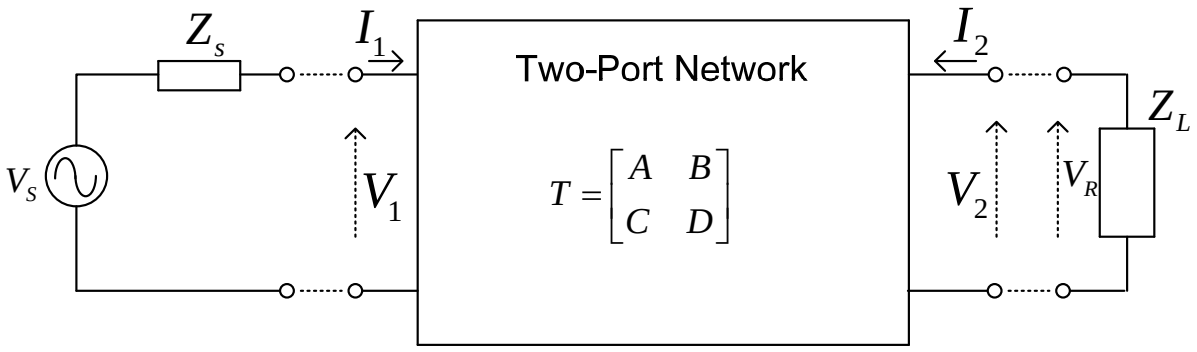

Fig. 4.10. Two-port Network Model for SPS BPL

$$\begin{bmatrix} V_1 \\ I_1 \end{bmatrix} = \begin{bmatrix} A & B \\ C & D \end{bmatrix} \begin{bmatrix} V_2 \\ I_2 \end{bmatrix} \tag{73}$$

$$\begin{bmatrix} V_2 \\ I_2 \end{bmatrix} = \begin{bmatrix} A & B \\ C & D \end{bmatrix}^{-1} \begin{bmatrix} V_1 \\ I_1 \end{bmatrix} \equiv \frac{1}{AD - BC} \begin{bmatrix} D & B \\ C & A \end{bmatrix} \begin{bmatrix} V_1 \\ I_1 \end{bmatrix} \tag{74}$$

Where $A = D = \cosh(\gamma l)$ per unit

$B = z_c \sinh(\gamma l)\ \Omega$

$C = 1/z_c \sinh(\gamma l)\ \ s$

$$V_S = V_1 + I_1 Z_S \tag{75}$$

$$V_R = V_2 = I_2 Z_L \tag{76}$$

$$H(f) = \frac{V_R}{V_S} = \frac{Z_L}{AZ_L + B + CZ_S Z_L + DZ_S} \tag{77}$$

Where Z_L is the receiver impedance

Z_S is the transmitter impedance

$$Gain(f) = 20.\log_{10}\left(\left|H(f)\right|\right) \quad (dB) \tag{78}$$

4.7 ESTIMATING THE CHANNEL THROUGHPUT CAPACITY

The transmission line channel is an inherently noisy and frequency selective fading channel. Channel coding on such channels is commonly performed using Orthogonal Frequency Division Multiplexing (OFDM) signal coding scheme[29]. It has been shown that OFDM can be modeled as a parallel Gaussian channel [30] which is a channel that has k independent Gaussian channels in parallel, with a common power restraint [31].

As illustrated in Fig. 4.11, the bandwidth of the distribution line channel is divided into k sub-bands. Each of these sub-bands make up an independent channel with input X_j and output Y_j and may have independent non-white Gaussian noise levels Z_j as shown in Fig. 4.12 and expressed in (79). Where the noise is described by the expression in (80). Thus, the distribution-line channel response, gain in (78), is divided into k Sub-channels of equal bandwidth, each with a different gain amplitude. The total BPL transmission power is distributed among all the Sub-channels, as expressed in (81),

to maximize the total capacity [31]. The total throughput capacity C of the distribution-line channel is the summation of the throughput capacity of each sub-channel with the optimum distribution of power to each sub-channel, while ensuring that the total transmission power is less than or equal to the total power constraint, as expressed in (82). For this work, the maximum gain amplitude available in each sub-channel was picked as the lowest amplitude within the sub-channel, as illustrated by the horizontal bars in Fig. 4.11.

$$Y_j = X_j + Z_j, \quad j = 1, 2, ..., k \tag{79}$$

$$Z_j \sim \mathcal{N}(0, N_j) \tag{80}$$

$$\sum_{j=1}^{k} EX_j^2 \leq P \tag{81}$$

$$C = \max_{f(x_1, x_2, ..., x_k): \Sigma EX_i^2 \leq P} I(X_1, X_2, ..., X_k; Y_1, Y_2, ..., Y_k) \tag{82}$$

Where X_j is the input power in each sub-channel
Y_j is the output power from each sub-channel
Z_j is the noise level in each sub-channel
P is the total signal transmission power
E is the Euclidean Sum
C is the total channel capacity in bit per second

The distribution that achieves the max throughput capacity of the channel needs to be calculated. Recall that the noise, $Z_1, Z_2, ..., Z_k$ in each sub-channel are independent, therefore, the information expression $I(X_j, Y_j)$ in (82) can be expressed as given in (83) to (86).

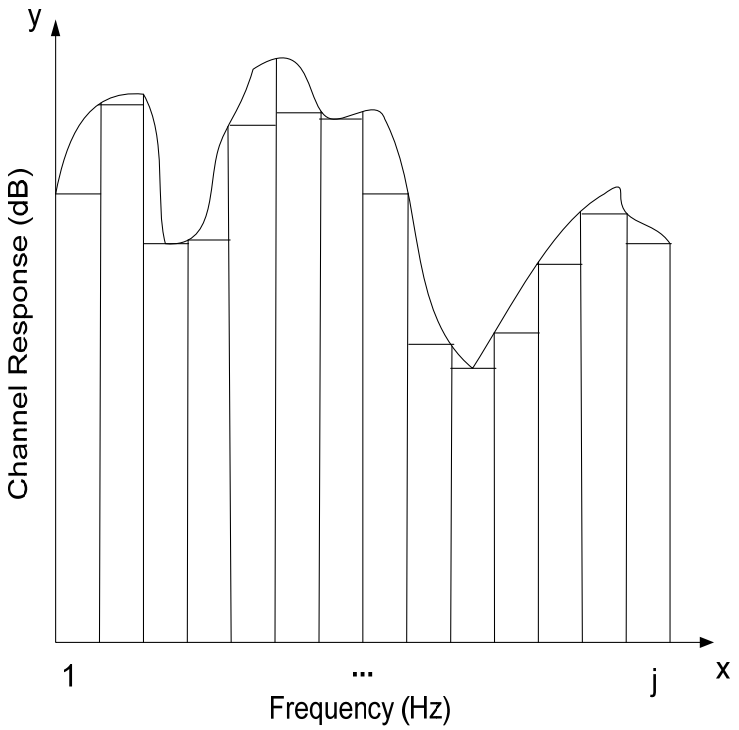

Fig. 4.11. Power Line Channel Divided into k Parallel Sub-channels

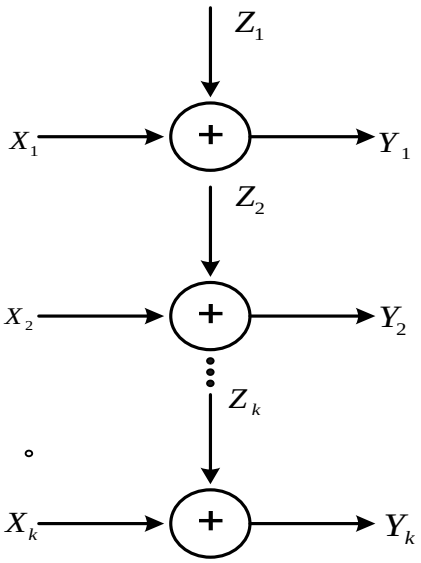

Fig. 4.12. Parallel Gaussian Channels [31]

$$I(X_1, X_2, ..., X_k; Y_1, Y_2, ..., Y_k) = h(Y_1, Y_2, ..., Y_k) - h(Y_1, Y_2, ..., Y_k \mid X_1, X_2, ..., X_k) \quad (83)$$

$$I(X_1, X_2, ..., X_k; Y_1, Y_2, ..., Y_k) = h(Y_1, Y_2, ..., Y_k) - h(Z_1, Z_2, ..., Z_k) \quad (84)$$

$$I(X_1, X_2, ..., X_k; Y_1, Y_2, ..., Y_k) \le \sum_j h(Y_j) - h\left(Z_j\right) \quad (85)$$

$$I(X_1, X_2, ..., X_k; Y_1, Y_2, ..., Y_k) \le \sum_j \frac{1}{2} \log\left(1 + \frac{P_j}{N_j}\right) \quad (86)$$

Where $P_j = EX_j^2$ and N_j is the noise variance in each sub-channel. There by reducing the problem to a standard optimization problem which can be solved using Lagrange multipliers [31]. The result of the optimization process is given in (87) and can be re-written as in (88), where v is the optimization factor. It should be noted however that the P_j's cannot be negative, as such the Kuhn-Tucker conditions is used to verify that the solution in (89) maximizes the capacity where v is chosen so that the power constraint is not violated, as expressed in (90). Thus, as the signal power is increased, power is first allotted to the channels with the lowest noise levels before residual power is allotted to noisier channels. This process is referred to as "water-filling" and is illustrated graphically in Fig. 4.13 [31].

$$\frac{1}{2} \frac{1}{P_i + N_i} + \lambda = 0 \quad (87)$$

$$P_j = v - N_j \quad (88)$$

$$P_j = \left(v - N_j\right)^+ \quad (89)$$

$$\sum\left(v - N_j\right)^+ = P \tag{90}$$

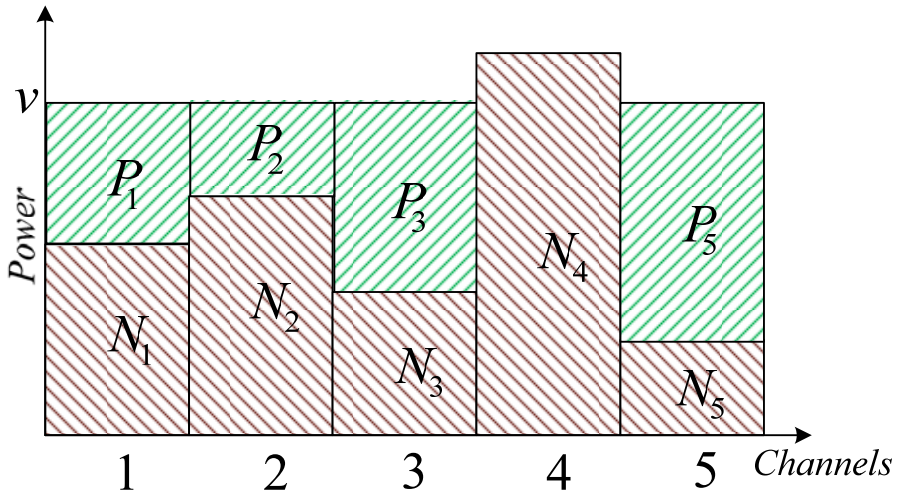

Fig. 4.13. Water-filling for parallel Channels[31].

4.8 SUMMARY

In this section, the development of the BPL/PLC channel model for shipboard power cables was discussed in detail. Using the MTL theory and TEM wave approximations, the decoupling of the propagating signals along the SPS transmission line was introduced. The decoupled differential signal propagating in the two excited phase conductors of the SPS transmission line make it possible to model the BPL/PLC channel of the SPS as a Two-conductor transmission line. The equivalent Two-port network representation of a Two-conductor transmission line is used to obtain the transfer function of the SPS power-line channel from which the frequency response of the channel can be calculated. A parallel Gaussian communication technique commonly

referred to as “water-filling” was also presented. The “water-filling” technique is used to estimate the channel throughput capacity of the SPS BPL/PLC channel from the obtained frequency response.

In the next section, a brief description of the implementation of the developed model will be presented. Some relevant concepts required to understand the principles applied in sections of the code will also be discussed.

5. IMPLEMENTATION

5.1 INTRODUCTION

This section discusses the implementation of the BPL/PLC channel characteristic model developed in the previous section. A brief description of a typical SPS power cable will be provided to clarify the input data required for calculating the primary line parameters. Cascading of Two-port networks to obtain an equivalent Two-port network model of the BPL/PLC power-line path will also be described. Finally, the structure of the Matlab code developed for performing the analytical model developed in Section 4 will be presented.

5.2 NOTIONAL NGIPS CABLES

A cross section view of a typical SPS Three-phase cable is shown in Fig. 5.1. The cable is comprised of three individually insulated conductor cores bound together using a filler and binder tape. An optional metal sheath, covered by a jacket, is provided for armored ship cables. The core conductor is usually made of coated or uncoated annealed copper depending on the manufacturer. A low-smoke, zero-halogen, flame retardant insulation and jacket material is used in shipboard cables to meet IEEE 1580 and Navy M24643 standards for use in marine applications. As seen in Fig. 5.1, the separation s of any two excited conductors is the sum of the radius of a conductor and twice the thickness of the conductor insulation.

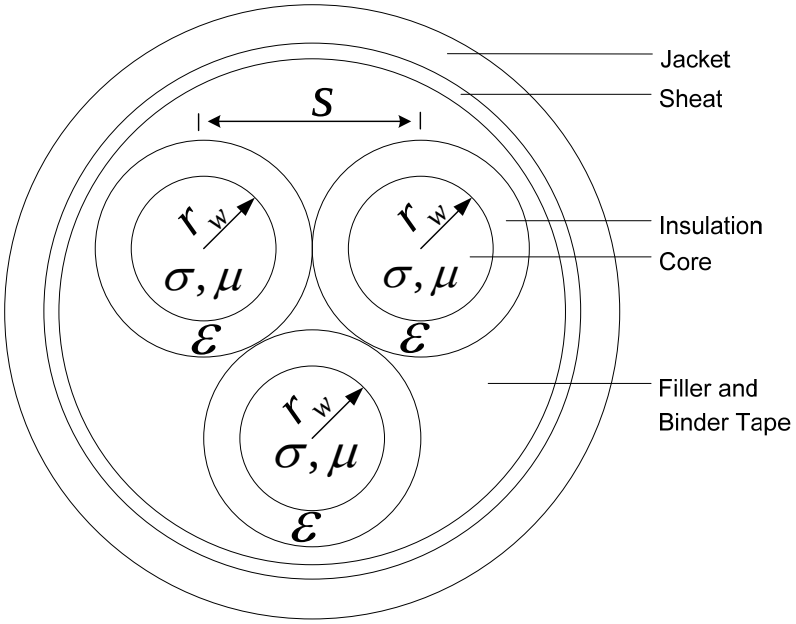

Fig. 5.1. Cross Section of Typical SPS Three-phase Cable

5.3 CASCADING TWO-PORT NETWORKS

In general, practical transmission lines contain bridged taps. A bridged tap is a branch line connection spliced unto the main transmission line as illustrated in fig xx a [32]. Each segment of the transmission line configuration in Fig. 5.2.a can be represented by its equivalent Two-port network model as shown in Fig. 5.2.b. The individual Two-port networks in this situation can be cascaded as shown in Fig. 5.2.c to obtain the overall Two-port network model of the channel. However, the ABCD matrix representation of the bridged tap Two-port network is of a different form shown in (91). Where Z_{inbt} is the input impedance of the bridged tap and can be calculated from the expression in (92). If the branch connection is unterminated (i.e. open circuit), the resultant input impedance is given in (93). The derivation of the matrix in (91) is given

in Appendix A. The ABCD matrix of the overall Two-port network shown in Fig. 5.2.d is obtained by multiplying the individual Two-port network matrices as shown in (94).

$$T_{bt} = \begin{bmatrix} 1 & 0 \\ 1/Z_{inbt} & 1 \end{bmatrix} \tag{91}$$

$$Z_{in} = \frac{AZ_L + B}{CZ_L + D} \tag{92}$$

$$\lim_{Z_L \to \infty} Z_{in} = \lim_{Z_L \to \infty} \frac{AZ_L + B}{CZ_L + D} = \frac{A}{C} \tag{93}$$

$$[T_{overall}] = [T_i] \bullet [T_{bt}] \bullet [T_{i+2}] \tag{94}$$

Where Z_L is the load connected at the second port of the Two-port network.

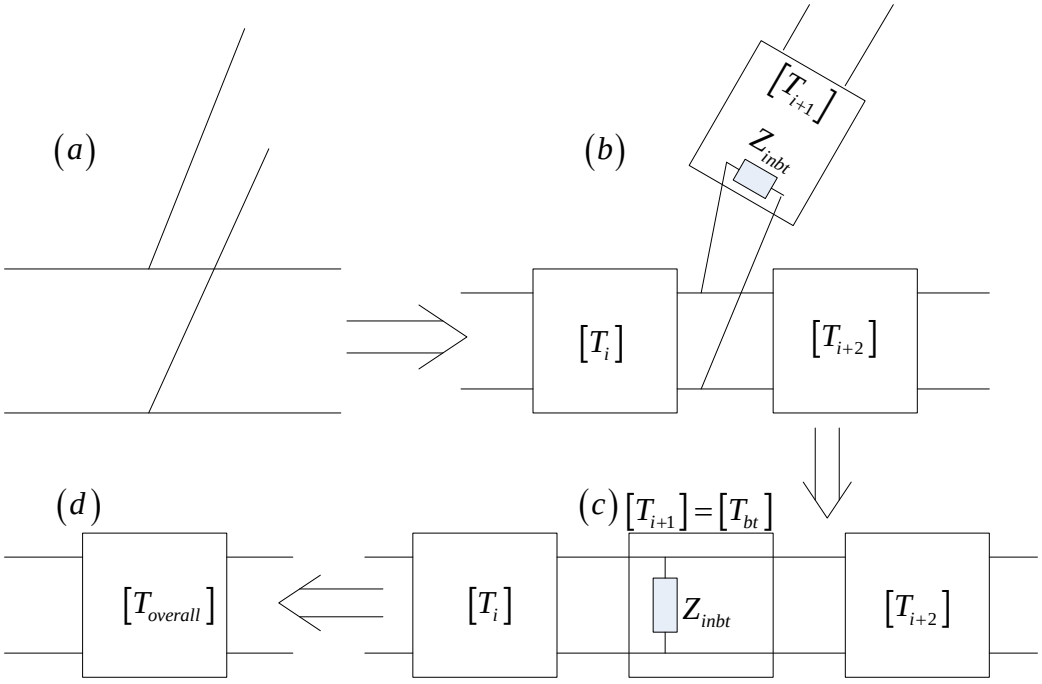

Fig. 5.2. Modeling Transmission Lines with Bridged Tap as a Two-port Network

5.4 MATLAB CODE FOR SIMULATING CHANNEL CHARACTERISTICS

The simulation code for examining the BPL channel response characteristics of the NGIPS series power system distribution lines was developed in Matlab. The Code was broken down into three functional blocks as illustrated in the flow chart in Fig. 5.3. The structure of each block will be briefly described in the following sub-sections.

5.4.1 Block A

In block A, the distribution line parameters Z_c and γ are calculated for each individual cable size, which were selected based on the voltage level and ampacity of each segment of the NGIPS architecture that make up the BPL path being considered. The cable specifications (radius r_w, separation s, core conductor conductivity σ, insulation permittivity ε, and permeability μ) from the manufacturers data sheet , for each cable size in the channel is used as input to block A. The distributed cable parameters R, L, G and C are then calculated for each cable and the results used to calculate Z_c and γ for each distribution line segment. This data is then stored in arrays and passed to block B.

5.4.2 Block B

The inputs to block B are the characteristics impedance Z_C and propagation constant γ for each distribution line segment. In block B, the equivalent Two-port network model for each distribution line segment is first calculated. The equivalent Two-port network model representative of the complete BPL channel path being considered is

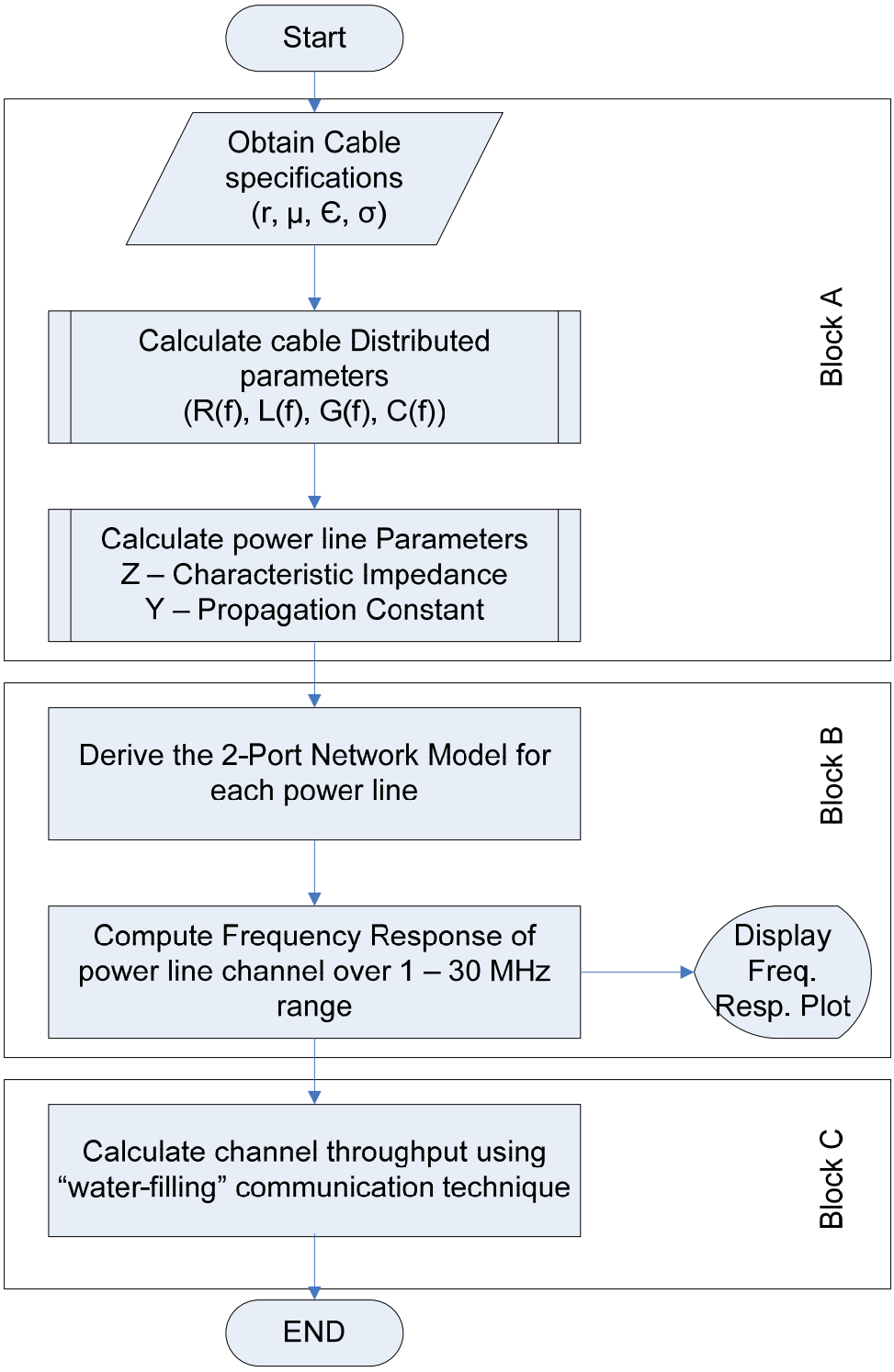

Fig. 5.3. Flow Chart of Analytical Model Matlab Code

then calculated by cascading the individual Two-port network models for each segment based on the specific topology of the BPL channel path. The transfer function of the channel is then calculated and the frequency response over the 1-30MHz range is calculated at a 1.5kHz interval. Finally, the frequency response data points from block B are stored in two columns in an excel file. First column gives the frequency points used and the corresponding channel response value in dB is stored in the second column.

5.4.3 Block C

Block C accepts the frequency response data points from the excel file created in block B as input. The total channel bandwidth, 29 MHz in this case, is divided into ‘k’ equally spaced Sub-channels based on user input specification. The power constraint variable is set to accept a range of values with a given step increase. These values are also to be set by the user. In this implementation, the channel noise in each sub-band is weighted by the inverse of the channel gain obtained in block B. This can be shown to be equivalent to weighting the input to each sub-channel by the gain in that channel. Mathematical proof of this is given in Appendix B. Using a binary search approach, the level of v that maximizes the throughput capacity of the BPL channel is then calculated for the power constraint range, at the specified intervals, provided by the user. The capacity for each sub channel is then calculated using the capacity equation in (88). Finally, the sum of these individual channel capacities is calculated and the result plotted and also stored in an excel sheet.

5.5 SUMMARY

The implementation of the analytical model developed for determining the BPL/PLC channel characteristics of the shipboard power cables was discussed in this section. The Matlab code structure used was divided into three blocks. The first block calculates the primary line parameters of the SPS cable. The results are then used in the second block to determine the frequency response of the SPS BPL/PLC channel. The third block performs the channel throughput capacity estimation of the SPS BPL/PLC channel.

The typical structure of a shipboard power cable, which identifies the cable parameters required by the first code block, was also discussed. This was accompanied by a discussion of the method of cascading Two-port networks which was used in the second code block to obtain the equivalent Two-port network model of the SPS channel. In the next section, some simulation studies performed using the code developed in this section will be presented.

6. SIMULATION STUDIES

6.1 INTRODUCTION

Simulation studies performed using the adapted BPL/PLC shipboard power cable channel model to investigate the frequency response characteristics of SPS transmission lines, are presented in this section. Some of the simulation cases presented were designed to investigate the channel response of theoretical automation paths based on the location of the component been monitored and the chosen location of the central control station. Other simulation cases designed to investigate the channel characteristics of individual SPS cables is also presented. The cable parameters used in these studies are given in Appendix C. Also, for the studies presented, the number of Sub-channels and the noise factor used were arbitrarily chosen as $k = 1000$ and $N_j = .01$ respectively.

6.2 PROPULSION SYSTEM AUTOMATION CHANNEL PATH

This case study was designed to determine the channel characteristic of the distribution line path linking a propulsion system and a potential central control station. A representative channel path from the notional NGIPS architecture shown in Fig. 3.3 was used in this study. In accordance with past practices on older generation ships, it was assumed that the central control station for monitoring the propulsion motor was served from a 450V AC load center node. The propulsion motor central control station in this study was assumed to be served within the lumped AC load in zone 3 of the NGIPS. The path from the propulsion motor PM1 to the lumped AC load center in zone 3 has

been indicated, on a cut section of the NGIPS, with thick dashed lines in Fig. 6.1. The equivalent channel path obtained is shown in Fig. 6.2.

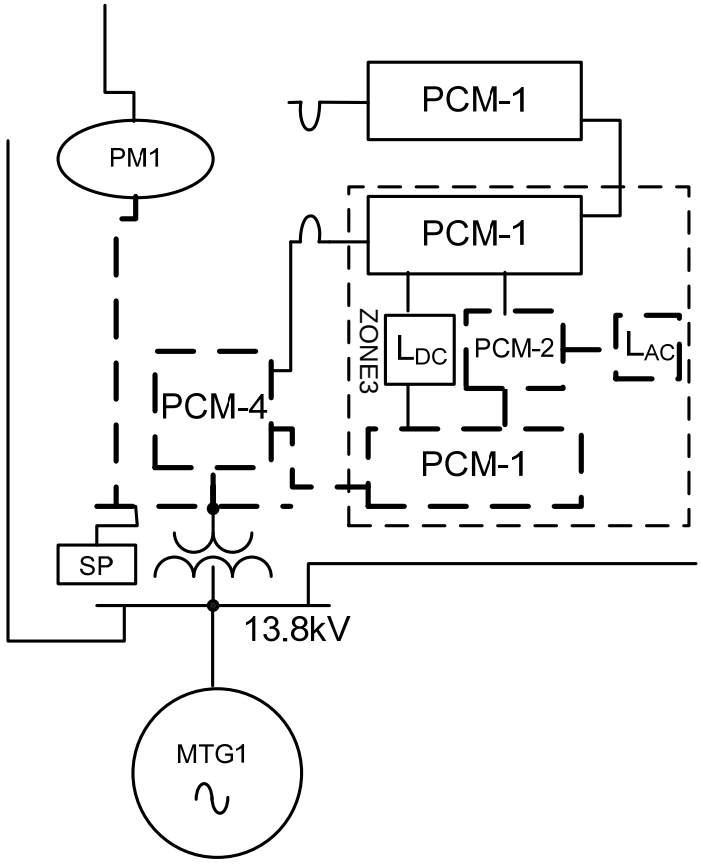

Fig. 6.1. NGIPS with PM1 Automation Path Shown

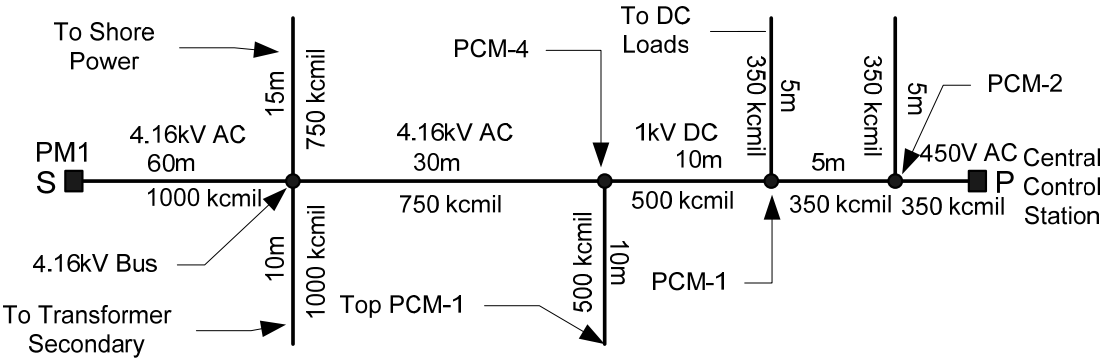

Fig. 6.2. SPS Channel between Propulsion System and AC Load Center

The length of each segment was an estimated value based on conceptual placement of individual components and the average size of a U.S. Navy ship. It should be noted that the other components in the system, such as the power converter modules, circuit breakers, switch boards, and bus transfers, were neglected in this study. The frequency response plot, showing the channel gain on the y-axis plotted over a 1-30MHz range, for the channel of Fig. 6.2 is shown in Fig. 6.3. The frequency selective nature of the SPS distribution line can easily be deduced from the sharp amplitude dips in the plot. A closer look also reveals that signal attenuation increases with the frequency as seen in the decreasing peak amplitude of the channel response as frequency increases. Fig. 6.4 is a plot of the estimated channel capacity of the channel. The estimated capacity, in mega-bits-per-second (Mbps), is plotted over an input signal power range of 10 to 100mW, which is within the range used in [6]. Fig. 6.4 shows a modest channel capacity of almost 50 Mbps at 100mW. However, from review of channel coding literature, it is believed that with various channel optimization techniques such as enhanced channel

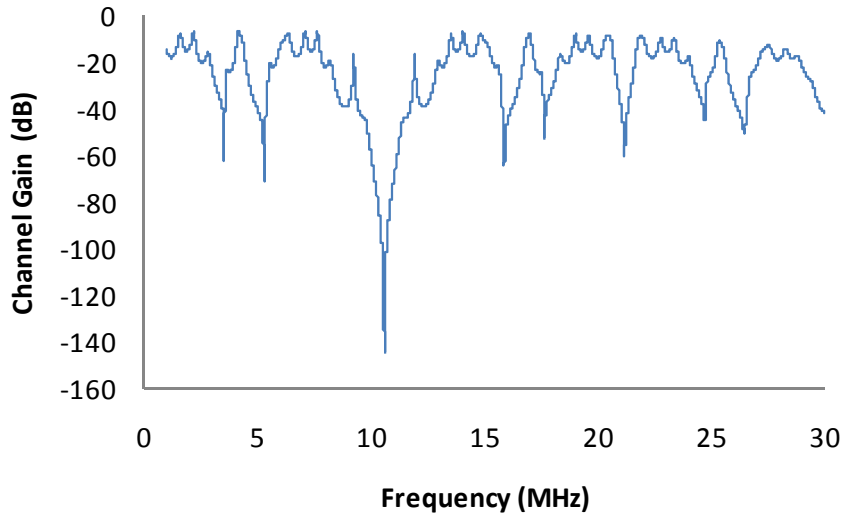

Fig. 6.3. Channel Gain for SPS Channel in Fig. 6.2

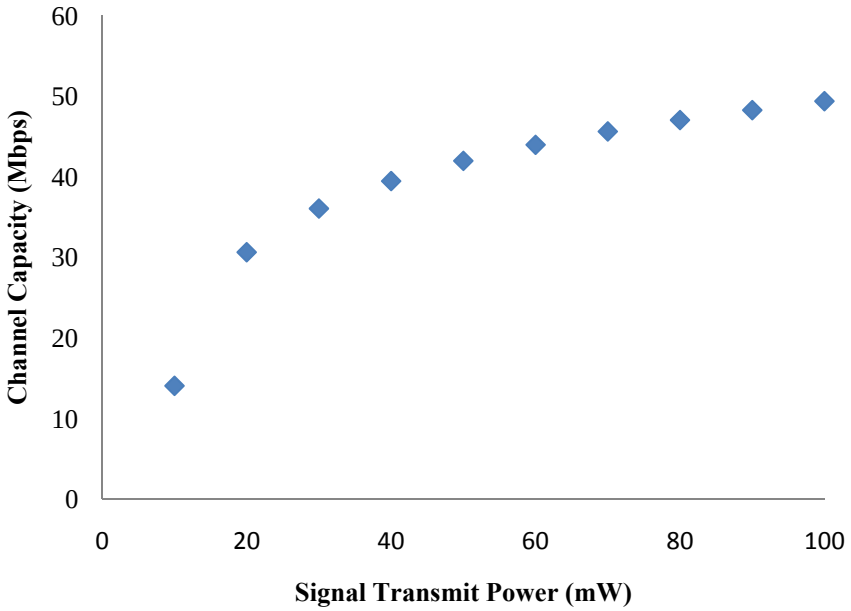

Fig. 6.4. Channel Capacity of SPS Channel in Fig. 6.2

coding and error correction, the capacity of the SPS distribution-line channel can be greatly increased.

6.3 CHANNEL CAPACITY FOR VARIOUS SIZES OF SPS CABLE

The purpose of this study was to investigate the channel capacity of different cable sizes, which were chosen based on the voltage and current levels in different parts of the notional NGIPS architecture. The frequency response for each cable size was calculated for 10m and 30m. The estimated channel capacity for each cable size and length was then calculated. The results of this study are shown in Table 1. In all, eight cable sizes for use at seven different voltage levels were considered over the two cable lengths, as shown in the first three columns, respectively. As seen, some cable sizes were used in multiple system voltage level applications. This is as a result of the ampacity in these applications for which multiple cable runs per phase are commonly used. The power constraint for the signal transmission level was varied between 10–100mW and the estimated channel capacity recorded.

The results obtained in Table 1 show that the channel capacity increases with the transmission power level. However, the relative capacity gain decreases with increase in transmission power. The results also show that the capacity of the channel reduces as the length of the channel increases. However, a clear pattern does not emerge based on the size of the cables.

.

Table 1. Table of Estimated Channel Capacity of Different Cable Sizes for Two Cable Lengths

Estimated Cable Channel Capacity (Mbps)												
Voltage (kV)	Cable Size (AWG/kcmil)	Length (m)	Signal Transmission Power Level (mW)									
			10	20	30	40	50	60	70	80	90	100
13.8	750	10	15.29	44.27	53.29	58.82	62.80	65.93	68.50	70.68	72.58	74.25
		30	15.16	44.06	53.08	58.60	62.58	65.71	68.27	70.46	72.35	74.03
	500	10	16.16	45.67	54.74	60.27	64.27	67.40	69.97	72.16	74.06	75.73
		30	16.04	45.49	54.55	60.09	64.08	67.21	69.79	71.97	73.86	75.54
4.16	1000	10	10.86	34.92	43.39	48.70	52.57	55.63	58.15	60.30	62.17	63.83
		30	10.73	34.53	42.97	48.27	52.14	55.19	57.70	59.85	61.71	63.37
	750	10	10.62	34.27	42.69	47.97	51.83	54.87	57.39	59.53	61.40	63.06
		30	10.50	33.88	42.26	47.53	51.38	54.42	56.93	59.07	60.94	62.59
1	500	10	12.92	39.81	48.64	54.09	58.04	61.14	63.70	65.87	67.75	69.43
		30	12.74	39.46	48.28	53.72	57.66	60.76	63.31	65.48	67.37	69.04
0.8	350	10	11.97	37.70	46.40	51.80	55.73	58.81	61.35	63.51	65.39	67.07
		30	11.79	37.31	45.99	51.38	55.30	58.38	60.92	63.08	64.96	66.62
	1/0	10	14.37	42.67	51.64	57.14	61.12	64.23	66.80	68.97	70.87	72.55
		30	14.14	42.29	51.25	56.75	60.72	63.84	66.40	68.58	70.48	72.15
0.65	350	10	11.97	37.70	46.40	51.80	55.73	58.81	61.35	63.51	65.39	67.07
		30	11.79	37.31	45.99	51.38	55.30	58.38	60.92	63.08	64.96	66.62
	4/0	10	12.47	38.86	47.64	53.07	57.01	60.10	62.65	64.82	66.70	68.37
		30	12.26	38.45	47.21	52.63	56.57	59.66	62.20	64.37	66.25	67.92
0.45	3/0	10	14.95	43.69	52.70	58.21	62.20	65.32	67.89	70.07	71.96	73.64
		30	14.75	43.37	52.37	57.88	61.86	64.99	67.55	69.73	71.63	73.30
	2/0	10	15.50	44.62	53.66	59.18	63.17	66.30	68.87	71.05	72.95	74.63
		30	15.30	44.32	53.35	58.87	62.86	65.99	68.55	70.74	72.63	74.31
0.375	1/0	10	14.37	42.67	51.64	57.14	61.12	64.23	66.80	68.97	70.87	72.55
		30	14.14	42.29	51.25	56.75	60.72	63.84	66.40	68.58	70.48	72.15

6.4 EFFECT OF LINE DISCONTINUITIES ON CHANNEL RESPONSE

This simulation study was setup to investigate the effect of distribution line discontinuities, due to series and parallel cable joints, commonly found in SPS distribution line networks. The frequency response and capacity of a simple distribution line of length 30m was calculated. Similarly, the frequency response of two distribution lines with cable sizes of 1000 kcmil and 500 kcmil, each 30m long and connected in series was calculated. The procedure was repeated using a 1000 kcmil distribution line segment 60m long with a segment of 500 kcmil distribution line 30m long spliced onto it at the 30m point. The frequency response plot for the simple line is shown in Fig. 6.5 and the corresponding channel capacity in Fig. 6.6. Fig. 6.7 shows the frequency response plot of the series discontinuity case and its corresponding channel capacity plot is shown in Fig. 6.8 while Fig. 6.9 and Fig. 6.10 show the frequency response and channel capacity plots of the branch discontinuity case respectively. It can be seen from the plotted graphs that the channel gain of the series discontinuity case is lower than that of the simple distribution line case. Furthermore, significant attenuation of alternate peaks can be seen in the series discontinuity frequency response plot. This is believed to be as a result of destructive reflections occurring at the point of discontinuity. Similarly, the channel response of the branch cable case is lower than that of the series discontinuity case. Also, significant frequency selective fading can be observed at about the 6 and 18 MHz bands in the branch discontinuity case. Overall, it was deduced that the channel frequency response and ultimately, the channel capacity, deteriorates with increasing number of discontinuities.

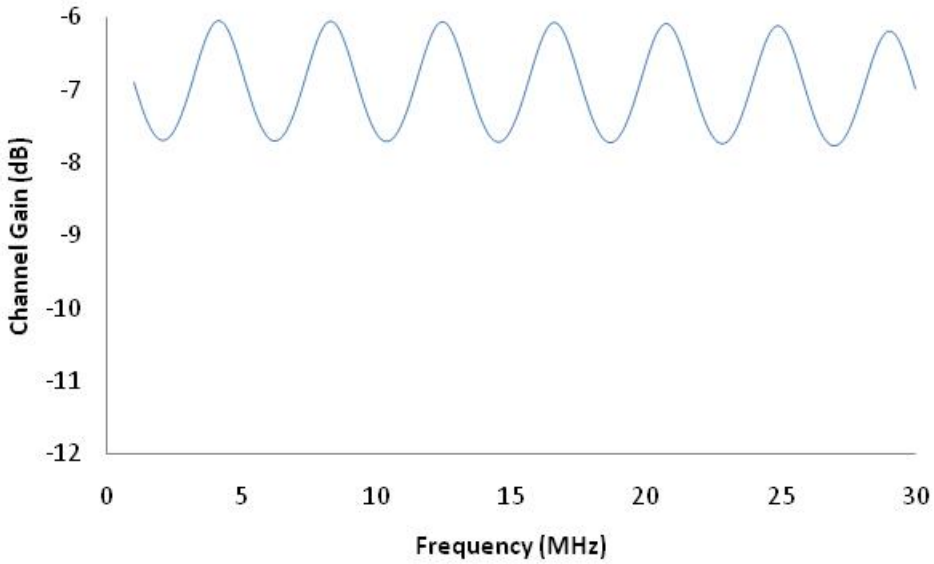

Fig. 6.5. Frequency Response Plot for Simple SPS Cable 30m Long

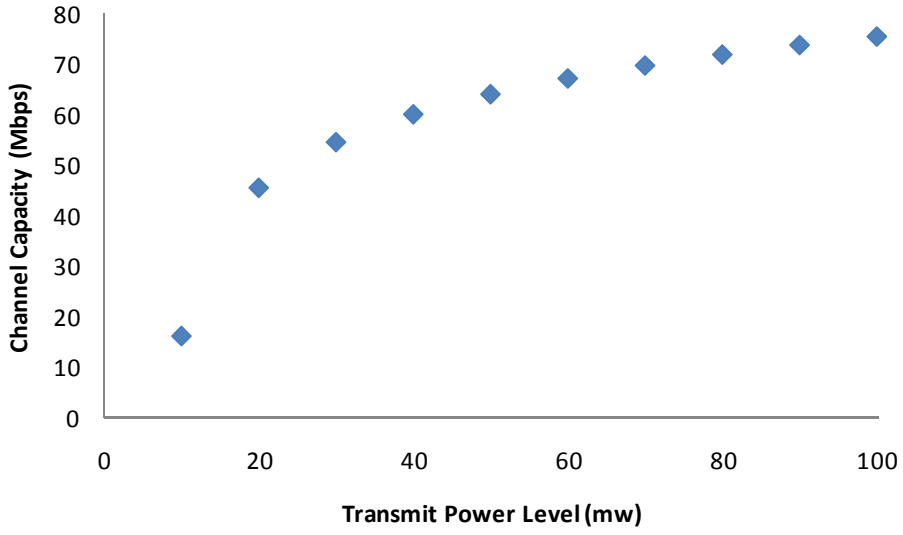

Fig. 6.6. Capacity Plot for Simple SPS Cable 30m Long

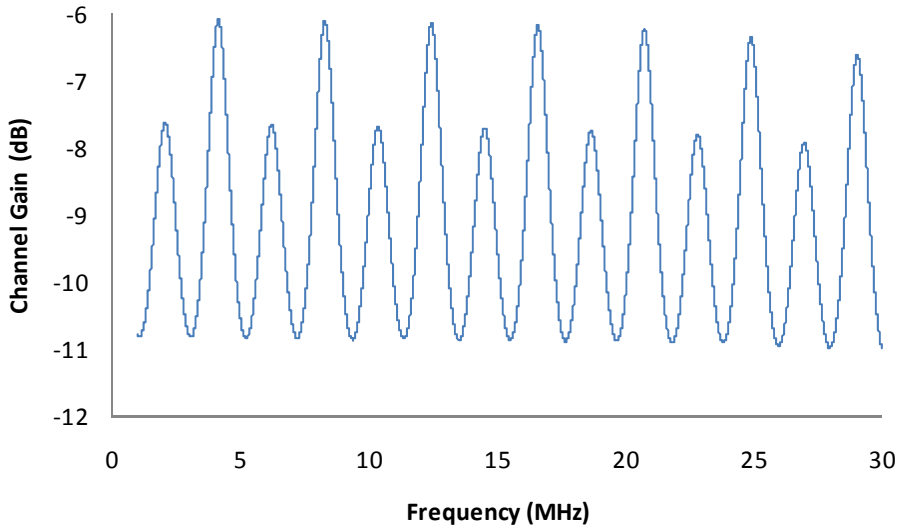

Fig. 6.7. Frequency Plot for Series Discontinuity of SPS Cable

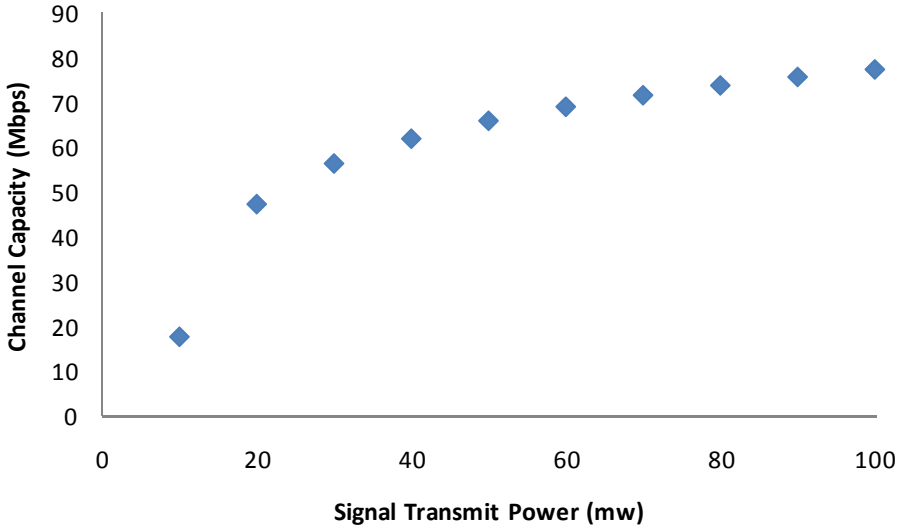

Fig. 6.8. Capacity Plot for Series Discontinuity of SPS Cable

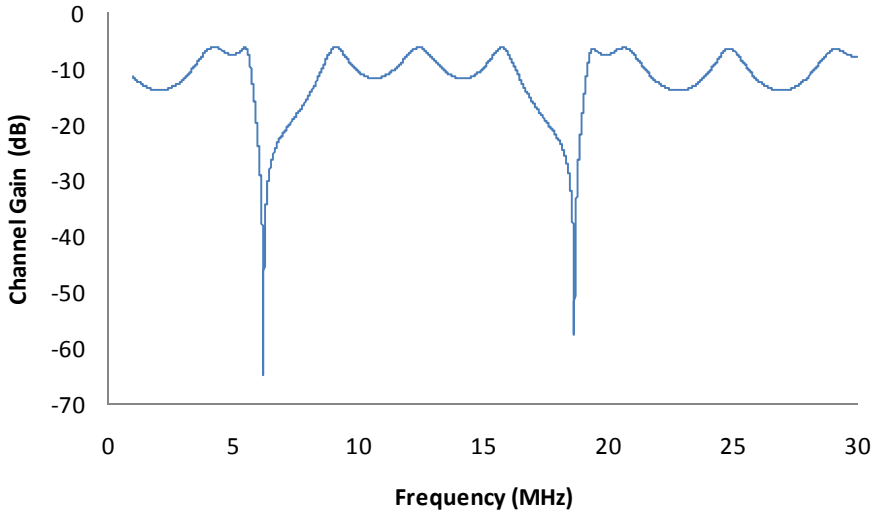

Fig. 6.9. Frequency Plot for Parallel Discontinuity of SPS Cable

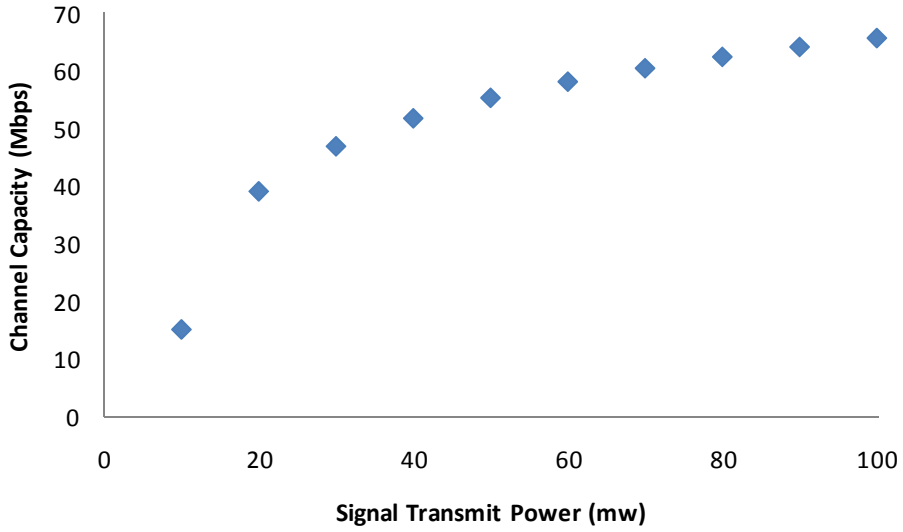

Fig. 6.10. Capacity Plot for Parallel Discontinuity of SPS Cable

6.5 SENSITIVITY STUDIES

Some sensitivity studies were performed to examine the influence of signal transmission levels, length of the cable channel, and the number of Sub-channels used. For the case presented here, the studies were performed for a 500 kcmil cable. To investigate the effect of power transmission levels, a fixed cable length of 50 m and a constant number (1000) of Sub-channels was used, while the transmit power level was varied from 1 mw to 200 mw. In the case of the examining the effect of the number of Sub-channels, the fixed cable length of 50 m was also used with a fixed transmit power level of 100mw, while the number of Sub-channels was varied from 100 to 2000. Similarly, the length of cable was varied from 10m to 200m while the signal transmit power level and the number of Sub-channels were held constant at 100mw and 1000 respectively.

The channel capacity plot with respect to cable length is plotted in Fig. 6.11. It can be seen from the trend in this figure that the capacity of the cable channel decreases almost linearly with increasing length of the cable. In Fig. 6.12, the plot of the channel capacity with respect to increasing power is shown. From this plot, it was deduced that the channel of the cable increases with increasing transmit power levels. However, the rate of increase in capacity with respect to transmit power can be seen to reduce with increasing power levels, indicating that a point will be reached where the opportunity cost of increasing power levels with respect to capacity may become unreasonable. Finally, the channel capacity plot with respect to the number of Sub-channels is given in Fig. 6.13. From this figure, the SPS channel capacity is seen to reduce non-linearly

with increase in the number of Sub-channels. However, the effect of the number of Sub-channels used is also dependent on the channel coding scheme used. As such, the author cannot make a decisive conclusion based on the results of this study.

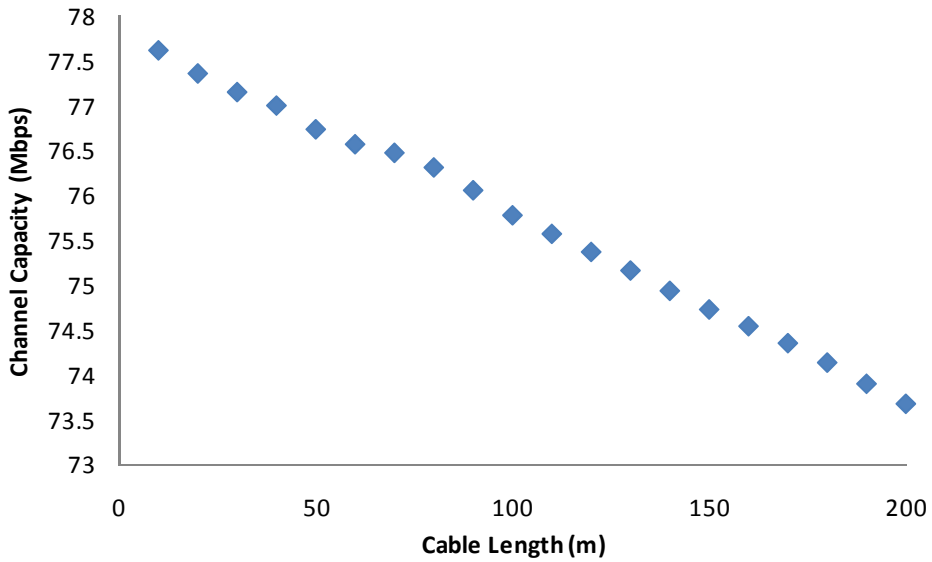

Fig. 6.11. Channel Capacity for 500 kcmil Cable at Varying Lengths with Constant Power (100 mw) and No. of Sub-channels (1000)

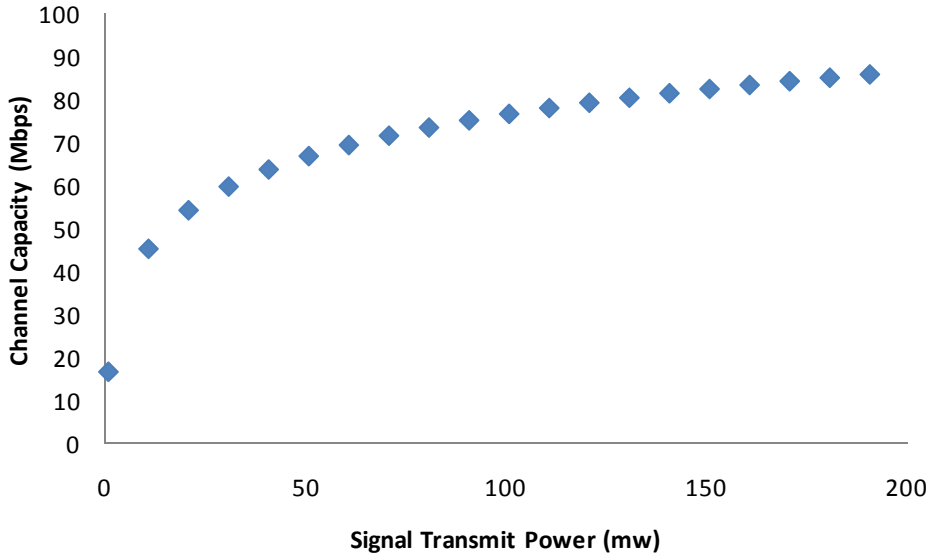

Fig. 6.12. Channel Capacity for 500 kcmil Cable at Varying Transmission Power with Constant Cable Length (50 m) and No. of Sub-channels (1000)

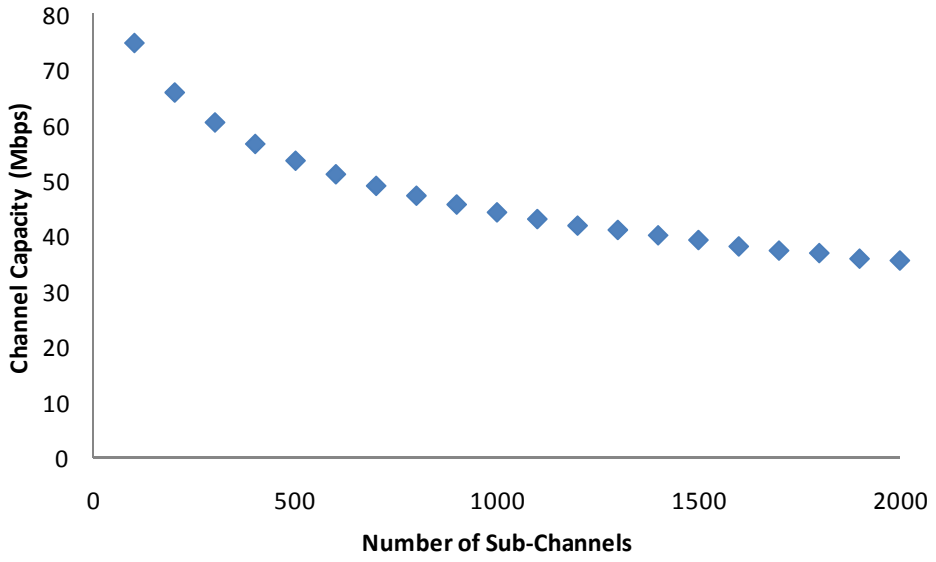

Fig. 6.13. Channel Capacity for 500 kcmil with Varying No. of Sub-channels with Fixed Power (100 mw) and Cable Length (50 mw)

6.6 SUMMARY

In this section, simulation case studies, assuming different scenarios, performed to investigate the channel response characteristics of the SPS distribution lines was presented. The case studies presented were designed to investigate the effect of distribution line length, distribution line discontinuities, signal transmit power level and number of Sub-channels. The channel characteristics of an hypothetical communication link for the automation of a propulsion motor was also presented. The results shown in this section indicate an estimated BPL channel throughput capacity of 10-74 Mbps which is comparable to broadband throughput capacity of some existing 10/100 Mbps wireless and Ethernet networks.

7. CONCLUSION

7.1 CONCLUSION

An analytical model for investigating the BPL channel response characteristics and estimated throughput capacity of U.S. Navy SPS distribution lines was presented in this paper. The SPS cable channel model was adapted from an existing MTL model for indoor residential power-line channels. An estimate of the channel throughput capacity of the SPS cables was obtained using a parallel Gaussian channel modeling technique. The results of simulation case studies were presented.

From the results, it was concluded that the distribution lines in the notional NGIPS U.S. Navy ships have comparable channel capacities, between 10 and 74 Mbps, for many broadband applications such as voice communications, music and video streaming. In general, the estimated channel capacities of the investigated cables obtained from the various simulation studies were low compared to the 100 Mbps physical layer capacity of existing 100baseT wireless and ethernet communication networks. However, with improved channel optimization schemes, the SPS distribution-line channel has great potential to attain higher speeds. Given the widespread existence of these distribution lines in the ship, there is significant potential for the application of BPL technology for use as communication networks for automation in NGIPS ships.

However, the analytical model was developed only for the SPS distribution lines in this work. Also, this model did not consider the effect of different voltage levels on the BPL signal. Thus, there is still a need to analyze the communication characteristics

of other SPS components, such as the power converter modules, bus transfers, and circuit breakers, to determine the feasibility of using the SPS as communications networks.

REFERENCES

[1] M. M. Islam, *A Guide to Electrical Installations on Shipboard*. New York, NY: Standards Information Network IEEE Press, 2004.

[2] J. C. Kim and E. I. Muehldorf, *Naval Shipboard Communications Systems*. Englewood Cliffs, NJ: Prentice-Hall, Inc., 1995.

[3] L. Er, G. Yangpo, G. Samdani, O. Mukhtar, and T. Korhonen, "Powerline communication over special systems", in *Proceedings of the 2005 International Symposium on Power Line Communications and Its Applications*, 2005, pp. 167-171.

[4] K. Talukdar, M. Stojanovic, and L. Freitag, "Through-the-hull acoustic communication technology - Ships hulls as a wireless medium for networking and data transfer among spatially distributed sensors", *Sea Technology*, vol. 47, pp. 45-49, May 2006.

[5] G. Held, *Understanding Broadband over Power Line*. Boca Raton, FL: Auerbach Publications, 2006.

[6] T. Esmailian, F. R. Kschischang, and P. G. Gulak, "In-building power lines as high-speed communication channels: channel characterization and a test channel ensemble", *International Journal of Communication Systems*, vol. 16, pp. 381-400, Jun 2003.

[7] S. E. Collier, "Delivering broad band internet over power lines: what you should know", in *Proceedings of the Rural Electric Power Conference, 2004*. 2004, pp. A1-1-11.

[8] J. Abad, A. Badenes, J. Blasco, J. Carreras, V. Dominguez, C. Gomez, S. Iranzo, J. C. Riveiro, D. Ruiz, L. M. Torres, and J. Comabella, "Extending the power line LAN up to the neighborhood transformer", *IEEE Communications Magazine*, vol. 41, pp. 64-70, 2003.

[9] C. Nunn and K. Sullivan, "From theory to practice: the development and implementation of PowerNet(R)-an advanced power line carrier system for AMR, DSM, DA and non-utility applications", in *Proceedings of the 14th International Conference and Exhibition on Electricity Distribution. Part 1. Contributions. (IEE Conf. Publ. No. 438)*. 1997, pp. 8/1-8/5 vol.5.

[10] P. van der Gracht and R. Donaldson, "Communication using pseudonoise modulation on electric power distribution circuits", *IEEE Transactions on Communications, [legacy, pre - 1988],* vol. 33, pp. 964-974, 1985.

[11] S. Tsuzuki, M. Yoshida, Y. Yamada, H. Kawasaki, K. Murai, K. Matsuyama, and M. Suzuki, "Characteristics of power-line channels in cargo ships", in *Proceedings of the IEEE International Symposium on. Power Line Communications and Its Applications, 2007. ISPLC '07.* 2007, pp. 324-329.

[12] S. Tsuzuki, M. Yoshida, Y. Yamada, K. Murai, H. Kawasaki, K. Matsuyama, T. Shinpo, Y. Saito, and S. Takaoka, "Channel characteristic comparison of armored shipboard cable and unarmored one", in *Proceedings of the IEEE International Symposium on Power Line Communications and Its Applications, 2008. ISPLC 2008.* 2008, pp. 7-12.

[13] T. Banwell and S. Galli, "A novel approach to the modeling of the indoor power line channel part I: circuit analysis and companion model", *IEEE Transactions on Power Delivery,* vol. 20, pp. 655-663, 2005.

[14] S. Galli and T. Banwell, "A novel approach to the modeling of the indoor power line channel-Part II: transfer function and its properties", *IEEE Transactions on Power Delivery,* vol. 20, pp. 1869-1878, 2005.

[15] H. Meng, S. Chen, Y. L. Guan, C. L. Law, P. L. So, E. Gunawan, and T. T. Lie, "Modeling of transfer characteristics for the broadband power line communication channel", *IEEE Transactions on Power Delivery,* vol. 19, pp. 1057-1064, 2004.

[16] N. Pavlidou, A. J. Han Vinck, J. Yazdani, and B. Honary, "Power line communications: state of the art and future trends", *IEEE Communications Magazine,* vol. 41, pp. 34-40, 2003.

[17] B. Hubscher, "Making broadband PLC a commercial reality", *Modern Power Systems,* vol.21, pp. 55-58, 2001.

[18] L. Yu-Ju, H. A. Latchman, L. Minkyu, and S. Katar, "A power line communication network infrastructure for the smart home", *IEEE Wireless Communications, [see also IEEE Personal Communications],* vol. 9, pp. 104-111, 2002.

[19] J. Walko, "Plug into data", *New Electronics,* vol. 39, pp. 18-19, 2006.

[20] A. J. Seman, III, "Next generation navy ship automation systems engineering from sensors to systems", in *Proceedings of the 2005 IEEE International Conference on Systems, Man and Cybernetics,* 2005, pp. 1218-1222 Vol. 2.

[21] Moxa, "Industrial Ethernet for in-ship communication." [Online]. Available: http://www.moxa.com/Zones/Industrial_Ethernet/Marine/Solutions.htm accessed on 5th January, 2008

[22] GlobalSecurity.org "Integrated Power System (IPS)" [Online]. Available: http://www.globalsecurity.org/military/systems/ship/systems/ips.htm accessed on 5th September, 2008

[23] C. R. Paul, *Analysis of Multiconductor Transmission Lines*. New York: Wiley, 1994.

[24] T. L. Baldwin and S. A. Lewis, "Distribution load flow methods for shipboard power systems", *IEEE Transactions on Industry Applications,* vol. 40, pp. 1183-1190, 2004.

[25] T. C. Banwell and W. E. Stephens, "Line code selection for 155.52 Mb/s data transmission on category 5 cable plant", *IEEE Journal on Selected Areas in Communications,* vol. 13, pp. 1670-1683, 1995.

[26] S. Galli and T. C. Banwell, "A deterministic frequency-domain model for the indoor power line transfer function", *Selected Areas in Communications, IEEE Journal on,* vol. 24, pp. 1304-1316, 2006.

[27] C. R. Paul, "Decoupling the multiconductor transmission line equations", *IEEE Transactions on Microwave Theory and Techniques,* vol. 44, pp. 1429-1440, 1996.

[28] C. R. Paul, *Introduction to Electromagnetic Compatibility*. New York: Wiley, 1992.

[29] M. Gotz, M. Rapp, and K. Dostert, "Power line channel characteristics and their effect on communication system design", *IEEE Communications Magazine,* vol. 42, pp. 78-86, 2004.

[30] S. Furrer and D. Dahlhaus, "Mean bit-error rates for OFDM transmission with robust channel estimation and space diversity reception", in *Proceedings of the International Zurich Seminar on Broadband Communications, 2002. Access, Transmission, Networking.* 2002, pp. 47-1-47-6.

[31] T. M. Cover and J. A. Thomas, *Elements of Information Theory*, 2nd ed. Hoboken, NJ: Wiley-Interscience, 2006.

[32] S. Galli and T. C. Banwell, "On the symmetry of the power line channel," in *Proceedings of the IEEE International Symposium on Power Line Communications and Its Applications* ISPLC'01, Malmo, Sweden, 2001, pp. 325-330.

APPENDIX A

Shunt Discontinuities in Transmission Lines

An example of a shunt discontinuity on a transmission line is shown in Figure 1. The voltages across the shunt resistance R_C is given in (95) with the voltage on the left side $V_1(b)$ at location b, equated to the voltage on the right side $V_2(a)$ at location a. In a similar manner, the current $I_1(b)$ at location b to the left of the resistor is given in (96). The ABCD matrix relating the voltage on the immediate left and right of the resistor is given in (99).

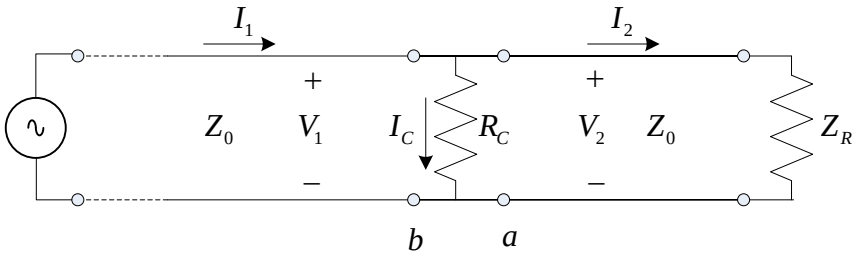

Figure 1..Shunt Discontinuity on Transmission Line

$$V_1(b) = V_2(a) \tag{95}$$

$$I_1(b) = I_C + I_2(a) \tag{96}$$

But,

$$I_C = \frac{V_2(a)}{R_C} \tag{97}$$

Therefore

$$I_1(b) = \frac{V_2(a)}{R_C} + I_2(b) \tag{98}$$

Writing equations (95) and (98) in matrix form yields

$$\begin{bmatrix} V_1(b) \\ I_1(b) \end{bmatrix} = \begin{bmatrix} 1 & 0 \\ 1/R_C & 1 \end{bmatrix} \begin{bmatrix} V_2(a) \\ I_2(a) \end{bmatrix} \tag{99}$$

APPENDIX B

In this appendix, the mathematical proof of the expression in (100) is given.

$$Y_i = AX_i + Z_i \equiv Y_i^{'} = X_i + {Z_i}/{A} \tag{100}$$

We will define ${Z_i}/{A} = Z_i^{'}$

From (9.67) of [31],

$$h(A\mathbf{X}) = h(\mathbf{X}) + \log|A| \tag{101}$$

From (10.68) of [31],

$$I(X_1, X_2, ..., X_k; Y_1, Y_2, ..., Y_k) = \sum_i h(Y_i) - h(Z_i) \tag{102}$$

Examining the right hand side of this equation and substituting $Y_i^{'}$ and $Z_i^{'}$, we get

$$h(Y_i^{'}) - h(Z_i^{'}) \tag{103}$$

$$= h\left({Y_i}/{A}\right) - h\left({Z_i}/{A}\right) \tag{104}$$

$$= h(Y_i) + \log\left|{1}/{A}\right| - h(Z_i) - \log\left|{1}/{A}\right| \tag{105}$$

$$= h(Y_i) - h(Z_i) \tag{106}$$

APPENDIX C

Table 2. Table of Cable Parameters

Voltage Level (kV)	Cable Size (AWG/kcmil)	Cond. Radius (mm)	Ins. Thickness (mm)	Seperation (mm)	Ins. Relative Permittivity	Ins. Relative Permeability	Conductor conductivity $(ohm\text{-}m)^{-1}$	Conductor Relative Permeability
13.8	750	12.32	5.59	23.5	3	1	5.95E+07	1
	500	10.16	5.59	21.34	3	1	5.95E+07	1
4.16	1000	14.1	2.92	19.94	3	1	5.95E+07	1
	750	14.05	2.79	19.63	3	1	5.95E+07	1
1	500	9.91	2.92	15.75	3	1	5.95E+07	1
0.8	350	9.6	2.41	14.42	3	1	5.95E+07	1
	1/0	5.31	2.03	9.37	3	1	5.95E+07	1
0.65	350	9.6	2.41	14.42	3	1	5.95E+07	1
	4/0	7.41	2.03	11.47	3	1	5.95E+07	1
0.45	750	12.57	3.681	19.932	3	1	5.95E+07	1
	3/0	5.97	2.543	11.056	3	1	5.95E+07	1
	2/0	5.33	2.543	10.416	3	1	5.95E+07	1
0.375	1/0	5.31	2.03	9.37	3	1	5.95E+07	1

VITA

Ayorinde Akinnikawe received his Bachelor of Science degree (summa cum laude) in electrical engineering in 2004 from Wichita State University in Wichita, Kansas. In January 2006, he entered the Electrical Engineering (Power) program at Texas A&M University in College Station and worked as a graduate research assistant at the Power System Automation Laboratory at Texas A&M University. He received his Master of Science degree in December 2008. His research interests include broadband over power lines and electrification of land transportation. Mr. Akinnikawe is a member of Eta Kappa Nu, ASME, and the National Society of Black Engineers.

Mr. Akinnikawe may be reached at Lauren Engineers and Constructor, Inc., 1200 Walnut Hill Lane, Suite 3950, Irving, TX 75038. His email address is akinnikawe@yahoo.com